1-1-2003

Residual stress analysis by digital spectral correlation

Shiwei (Stanley) Ma
Ryerson University

Residual stress Analysis by Digital Speckle Correlation

By

Shiwei (Stanley) Ma

A project report

presented to Ryerson University

in partial fulfillment of the

requirement for the degree of

Master of Engineering

in

Mechanical, Aerospace, and Industrial Engineering

Toronto, Ontario, Canada, 2003

Author's declaration

I hereby declare that I am the sole author of this project.
I authorize Ryerson University to lend this project to other institutions or individuals for the purpose of scholarly research.

Signature

I further authorize Ryerson University to reproduce this project by photocopying or by other means, in total or in part, at the request of other institutions or individuals for the purpose of scholarly research.

Signature

Borrower's Page

Ryerson University requires the signatures of all persons using or photo copying this thesis. Please sign below, and give address and date.

Abstract

Residual stress is the stress which exists in the bulk of material without application of an external load and it is self-equilibrating. The resultant force and the moment which they produced must be zero. The formation of residual stress can be from primary product, surface removal, joining, mechanical surface treatment and heat treatments.

Residual stress is an important characteristic in engineering design because it can have a significant influence on the fatigue lives of engineering components which can also be both detrimental and beneficial. Extensive case studies regarding autogrettage, cold expansion, shot peening, laser shock peening and low plasticity burnishing have been examined and analyzed, so as to show that residual stress can be induced intentionally and unintentionally.

As to determine the residual stress, various quantities and qualitative methods have been introduced, which can be distinguished between destructive techniques such as the hole drilling method, the ring core technique, layer removal method and the sectioning method and the non-destructive techniques are including X-ray method, the neutron diffraction method, the ultrasonic techniques, magnetic Methods and Raman Spectroscopy.

A classical method of measuring residual stress is to use hole drilling in combination with strain gages. However, the strain gages inherent nature gives it a disadvantage when used to measure the residual stress. This disadvantage may be eliminated through the implementation of the Digital Speckle Correlation method (DSC). DSC is a computerized method which determines the displacement, strains and consequently calculates the stress. Thus this project demonstrates the viability of hole drilling in combination with DSC.

The DSC technique has been examined and many measurement parameters and factors have been discussed and analyzed. The recommendation has been made to provide a

straightforward solution. The parameters and factors include range determination, depth determination, principal direction determination, convergence area in the stress graphics and full coverage of measurement field.

Based on the Kirsch solution, the relationship between the biaxial residual stress and the released strain components has been derived. Consequently, the relationship between the released strain and residual stress has been established. With the aid of MathCad 8, the visual contact can be shown the relation, which provides a better understanding of the determination of residual stress by DSC method.

Acknowledgements

"Propose question, analyze the question, solve the question"_____ Zedong Mao, spirit leader, philosopher, poet and former president of PR China.

I would like to give my thanks to my supervisor Professor Hua Lu, who provided the consistent help in the whole project, my wife who supported my whole life in this period of time, my mother and my father who kept showing me the light from the overseas and Mr. Abuzar Ali who gave me financial support, without them this work would not have been possible. This project is for them.

Table of Contents

Nomenclature

γ_m	Maximum shear strain
$\gamma_{R\Theta}$	Shear strain in (R, Θ) coordinate
γ_{XY}	Shear strain in (X,Y) coordinate
ε_a	Initial residual average normal strain
ε_a'	Hole drilling released average normal strain
ε_R	Residual redial normal strain
ε_X	Residual normal strain in the X direction
ε_Y	Residual normal strain in the Y direction
ε_x	Residual normal strain in the x direction
ε_y	Residual normal strain in the y direction
ε_X'	Hole drilling released normal strain in X-direction
ε_Y'	Hole drilling released normal strain in Y-direction
ε_R'	Hole drilling released radial strain
ε_Θ'	Hole drilling released tangential strain
Θ	Angle between (X,Y) and (R, Θ)
θ	Angle between (x,y) and(r, θ)
Θ_p	Angle between (X,Y) and (x,y)
σ_r''	Radial stress in (r, θ) after hole drilling
σ_R''	Radial stress in (R, Θ) after hole drilling

σ''_{Θ} Radial stress in (R, Θ) after hole drilling

σ''_{θ} Radial stress in (r, θ) after hole drilling

σ_1 Initial Residual principal stress

σ_2 Initial Residual principal stress

σ'_a Hole drilling released average normal stress

σ_r Initial residual radial stress in (r, θ)

σ_R Initial residual radial stress in (R, Θ)

σ'_r Hole drilling released radial stress in (r, θ)

σ'_R Hole drilling released radial stress in (R, Θ)

σ_{Θ} Initial residual tangential stress in (R, Θ)

σ'_{Θ} Hole drilling released tangential stress in (R, Θ)

Initial residual tangential stress in

σ'_{θ} Hole drilling released tangential stress in

$\tau''_{r\theta}$ Shear stress in (r, θ)after hole drilling

$\tau''_{R\Theta}$ Shear stress in (R, Θ)after hole drilling

τ_m Maximum shear stress

$\tau_{r\theta}$ Initial residual shear stress in (r, θ)

$\tau_{R\Theta}$ Initial residual shear stress in (R, Θ)

$\tau'_{r\theta}$ Hole drilling released shear stress in(r, θ)

$\tau'_{R\Theta}$ Hole drilling released shear stress in(R, Θ)

	Young's Modules
ν	Poisson's Ratio
ω	Rigid Body Rotation

Chapter 1 Introduction

Residual stress is the stress which exists in the bulk of material without application of an external load (applied force, displacement of thermal gradient). All residual stress systems are self equilibrating, the resultant force and the moment which they produce must be zero.[1]

Residual stress is produced by heterogreneous plastic deformation, thermal contractions and phase transformations induced by the manufacturing process. These compressions are compensated by tensile stresses in the bulk of the sample. Most manufacturing processes and surface treatments produce residual stresses such as:

- Primary product: casting, forming, forging, drawing, extruding, rolling, spinning, bending, etc;
- Surface removal: machining, electro-erosion, etc;
- Joining: welding, brazing, etc;
- Mechanical surface treatment: shot peening, laser shock, etc;
- Heat treatments, chemical and thermochemical treatments: quenching, carburizing, etc.

Therefore, it comes to the challenge of how to determine the residual stress. Many available mathematics methods can be used and several techniques can be operated accordingly. Details of the technique will be discussed, compared and concluded in the later chapters. One of the techniques named Digital Speckle Correlation method (DSC) used by the author has been introduced and the mathematics relationship between the biaxial residual stress and the released strain components have to be established in order to obtain the result.

Consequently, the equation of released strain components in term of the residual stress is formed. The visual contact has been made to express the best understanding the relationship between the residual stress and released strain components.

Chapter 2 Influence of Residual Stress

Residual stress can have a significant influence on the fatigue lives of engineering components. Up to present, it is known that the near surface tensile residual stress tends to accelerate the initiation and growth phases of the fatigue process while the compressive residual stress close to the surface may prolong fatigue life. The residual stress can be induced intentionally and unintentionally and the influence of it can also be either detrimental or beneficial. For the purpose of an accurate assessment of fatigue lifetime, a detailed knowledge of residual stress including the magnitude and direction is required.

Current study indicates that fatigue accounts for at least ninety percent of all service failures due to mechanical cause. Among all the factors that cause the fatigue, the residual stress is one of the factors that is not easily noticed and sometimes not even realized by people.

In this case study part, some surface processes that intentionally introduce the beneficial stress to the sample surface including autofrettage, cold expansion, shot peening, laser shock peening and low plasticity burnishing are discussed. Afterwards, the test shows that fatigue life of the samples has been prolonged significantly.

2.1 Autofrettage

Autofrettage is the process by which beneficial residual stress introduced into thick-walled tubes by initially subjecting the tube to high internal pressure that causes plastic deformation. As a result, loads carrying capacity of the tube is increased due to the presence of residual stresses, this process also enhances the fatigue life of the tube.

Under the application of the Autofrettage process, the bore undergoes plastic deforemation. When the

pressure is released, the plastic deformation of the bore is maintained, while the deformation of the outside portion of the tube is recovered to nearly its original position. This non-uniform recovery results in compressive residual stress at the bore and tensile residual stress at the outside radius. [3]

The tangential compressive residual stress in the core suppresses crack formation, resulting in fatigue life improvement. As mentioned above, the distribution of residual stress is needed to be determined, which was calculated by using an elastic-plastic finite element stress analysis.

In the study reported by Pu and Hussain[4], they suggested that an active thermal loading could produce elastic thermal stressed equivalent to the autogrettage residual stress in a partially autofrettaged thick-walled pressure vessel. Based on this, the thermal loading was used as the input data in the residual stress analysis. The keyway grooved objective has been examined and the results showed the compressive stress at the bore region and stresses became tensile through the thickness, while at the root of the groove, the residual stress increased in order to evaluate the fatigue life.

The load-controlled simulation fatigue tests were conducted. The results showed that firstly, during the test, the considered crack initiation life of 2 mm crack length formed at the all corners of the specimens, as expected. Secondly, the lower level of the autofrettage is, the longer the fatigue life last.

It implies that the fatigue life of pressure vessel is influenced by the magnitude of tensile residual stress. The local stress and local strain estimate by both elastic-plastic finite element analysis and Neuber's rule were used in predicating the fatigue life, the results are reasonably in agreement with the experiment result.

In Thumser's paper [5], the autofrettage process by 10 kbar has been tested on the ASIS 4140 steel samples and the endurance limit has been improved by a factor of 2.4. He concluded that the higher compressive stresses result in higher endurance limit. Furthermore, prediction accuracy might suffer

for components with weaker notches.

2.2 Cold Expansion

The most effective and widely accepted method of fastener hole expansion in the aerospace industry is the split-sleeve process introduced by fatigue technology incorporated[6]. The survey shows that the main source of fatigue damage in the aircraft structure is fastener holes. The study [7] shows that seventy percent of fatigue cracks originated from the holes of riveted or bolted joints.

The hole cold expansion has been employed for over forty years. This involves pulling an oversize tapered mandrel through an internally lubricated expandable split-sleeve inserted into the hole. The sleeve prevents direct contact between the sliding mandrel and the hole, reducing damage to the inside of the hole and minimizing the material flow through the thickness direction. Consequently, the maximized compressive hoop stress at the periphery of the hole may further increase with the degree of cold expansion, which mainly limit by available tooling.

The residual stress zone acts to retard crack growth around the hole, thereby increasing the fatigue life of the component. This process can improve the fatigue life by 3-10 factor in the simple specimens subjected to constant amplitude loading. [8]

Because fatigue cracks tend to initiate at fastener holes particularly in highly stressed areas such as the bottom skins of wings, the fastener hole is expanded by pulling an oversize mandrel through it. The surrounding material is left compressed retarding or arresting crack growth. The result shows that the mean lives for Cx and NCx specimens and the life improvement factors have been significant longer.

The comprehensive three-dimensional elastic-plastic finite element analysis[9] was conducted to evaluate the development and growth of the plastic zone and unloading residual stress resulting from

the cold expansion of interacting adjacent fastener holes. The contact between the mandrel and the hole was modeled using special contact elements, which employ the combined penalty-Lagrange multipliers formulation. The results were the used to predict fatigue crack growth in the presence of residual stress using a specimen containing two holes in close proximity.

The X—ray and Garicai-Sachs methods[10] were used to measure the residual stress in the cold expanded hole before and after exposure to the high temperature. The result shows that exposure to temperature alone leads to a relaxation of residual stresses induced by cold expansion of fastener holes, the larger the magnitude of the residual stress, the larger the relaxation. The benefits derived from the cold expansion were significantly reduced at both 20 °C and 150 °C. The reduction in fatigue life improvement factor was even larger at 150 °C compared to 20 °C .

2.3 Shot Peening

Shot peening method is first developed by Kobayashi [11]. Shot peening is a cold working process used mainly to improve the fatigue life of metallic components. The results are accomplished by bombarding the surface of the component with small spherical shots made of hardened cast steel, conditioned cut wire, glass or ceramic beads at a relatively high velocity.

After contact between the target and the shot has ceased, a small plastic indentation is formed causing stretching of the top layers of the exposed surface. Upon unloading, the elastically stressed sub-surface layers tend to recover their original dimensions, but the continuity of the material in both zones, the elastic and the plastic, does not allow this to occur. Consequently, the compressive residual stress fields is highly effective in preventing premature failure under conditions of cyclic loading.

Besides, a study has been conducted regarding the dynamic elastic-plastic analysis of the process using a single shot. Specifically, it is desired to evaluate the effect of shot velocity, size and shape

upon the time variations of the contact force, the velocity history, the plastic zone developments and its growth and unloading residual stress.

In industries, shot peening is controlled with the help of Almen plates. They are standardized thin plates that are placed in parallel to the treated material, receiving the same treatment. This treatments induced residual stress in small plates that become deformed. It results in hardened surface layers of material in which the compressive residual stress can stop or at least slow down the initiation and propagation of the fatigue cracks.[12,13,14] This deflected shape caused by the process is called Almen intensity and its value is appropriate to adjust the shot peening parameters.[15]

Torres and Voorwald induced the residual stress by the shot peening to the AISI 4340 steel which is widely used steel in the aircraft and automobile industry. Both finite element analysis and the empiric model based on the experiment data. [16, 17] The specimens are treated with four intensities of shot peening: 0.0027A, 0.0063A,0.0083A and 0.0141A. The residual stress induced was measured by X-ray diffraction method with Raystress equipment.

The S-N curves for the base material and four peening conditions are plotted and showing the improvement in the fatigue resistance of the specimens with shot peened compared to the base material. However, it is noted that the best fatigue life condition was found in the intermediate peening condition rather than in the highest or lowest peening condition. They also concluded that the greater the peening intensity, the greater width of the compressive residual stress field. However, the surface residual stress was independent of the peening conditions.

In the high cycle, the shot peening pushed the crack sources beneath the surface, while in the low cycles, the cracks originated from the surface. According to the statement of Li , Zhang and Yao [14], the surface stresses are more related to the mechanical characteristic such as hardness and elastic recuperation and surface condition than to the shot peeing intensity. Therefore, it is concluded that the

improvement in fatigue life is a consequence of the compressive stress field induced by the shot peening.

Limitation of shot peening

Solid shot cannot always penetrate the most inaccessible areas of a component. For very small radius the process in limited to the depth of compressive stress achievable [18]. In practice shot peening parameters are specified to ensure that the depth of compressive stress from any surface penetrated no greater than 10 % of the section thickness. This becomes a problem on very thin components such as gas turbine compressor blades and plate valves. Care must also be taken to ensure that the shot peening intensity is controlled to ensure that the compressive stress is optimized at the surface.

Further, the solid shot cannot always penetrate the most inaccessible lasers of the components. Shot of no greater diameter than half the highest radius on the component should be utilized to ensure adequate coverage. For very small radius the process is limited to the depth of compressive stress achievable.

2.4 Laser Shock Peening

In laser materials processing such as laser machining, target material inevitably undergoes intensive non-uniform temperature change and as a result a complex residual stress distribution forms near the processed areas. An unfavorable stress distribution may result in micro crack formation and propagation, reduce the part's fatigue life and lead to catastrophic failures.

Laser shot peening (LSP) has been studied on and off since 1970s, in which laser generated shock waves in a confining medium are used to improve the mechanical properties of metallic material

including aluminum, steel and copper alloys, In particular, LSP induced compressive residual stress in the target and improves its fatigue life, lasers of 1.06μm wavelength and 1-6 mm beam size are commonly used in conventionally LSP. [19]

The basic principle is explained as follows. First, a high energy pulsed laser beam onto the surface of the part. A dual component overly is applied to the surface over the area. It consists of a thin film of material opaque to the laser beam, which is placed directly on the surface. The second is thicker film, transparent to the laser beam, which is over the first layer.

When the laser beam strikes the material, it passes through the transparent film (thicker one) and absorbed by the opaque film (the thinner one), caused the thin film to vaporize, The rapid expanding, heated gas is confined on the surface of the metal part by the thicker layer, creating pressures of 6 GPa. This surface pressure propagates into the parts as a shock wave, the high residual surface compressive stress is produced. The schematic of laser shot peening process is shown as follows in the figure 2-1:

Figure 2-1 Laser shot peening schematic

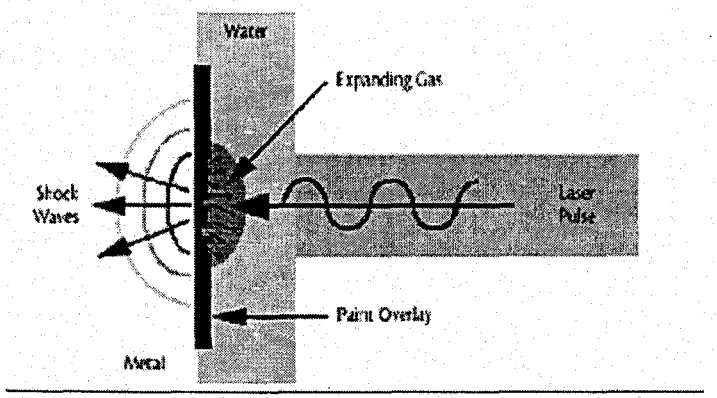

The coating could be metallic foil, organic paints or adhesives. These coatings can modify the surface loading transmitted to the substrate by acoustic impedance mismatch effects at the coating-substrate interface, and additional fifty percent increase in the peak stress values can be achieved.

Water is used to physically constrain the gas release, the advantages of using water as medium is that

it can reduce heat affected zone and focus the beam. However, the overly high laser intensity may cause water breakdown. When water breakdown takes place, laser energy cannot reach the target surface efficiently and water will lose its function of confinement, the exact level of laser intensity causing water breakdown depends on laser wavelength and laser water interaction time. Since the great interest is fatigue life and fatigue strength, it can reduce fretting fatigue and stress-corrosion cracking.

Earlier modeling work on laser-induced shock waves was carried out by Clauer[19]. Their model considered the non-linear coupled irradiation and hydrodynamic equations governing pressure evolution at the metal surface. Fabbro[20] developed a model which assumed that the laser irradiation is uniform and therefore shock propagation in the confining medium and the target. The assumption is appropriate when the size of laser beam which typically follows a Gaussian distribution, is relatively large. The shock model in this paper made modifications to Fabro's model assuming the laser beam spot size is in the order of microns.

The governing equations for stress analysis follow standard elasticity-plasticity analysis except the extremely high pressure and strain rate involved for especial considerations. The influence of the high strain rate on the yield strength of material has been considered.[21] The influence of pressure on the yield strength of material was found to be more important than other effects when the pressure was given by Steinberg. Steinberg's model did not consider rate dependent effects. For shock pressures below 10 GPa, the rate dependent effects cannot be neglected. In laser shock processing, the pressure involved is fairly high but less than 10 GPa. Therefore, both strain rate effects and shock pressure effects on the yield stress of materials need to be considered.

From Peryre [22] research paper, laser shot peening is a very attractive, promising, new surface treatment for aluminum alloys yielding large fatigue improvements in A 356, A112Si and 7050 alloys. In this study, mechanical surface modifications were investigated to the residual stress field induced,

surface hardening and surface roughness modifications. In all three alloys investigation, the residual stress fields extend to a greater level. Hardening is limited to +10% of the initial value, which is half of the increase achievable by conventional shot peening treatment. The main difference between two treatments has been demonstrated: laser shot peening generated a general compression of the material with no roughness changes; shot peening strongly affects the surface and created potential initiations sites. Much better fatigue performance is observed with laser shocked 7075 than with conventional shot peened specimens. This is attributed, through fatigue crack detection to large increases in the crack initiations stage for laser shot peening than for shot peening specimens. It has also been shown that a combination of laser shot peening and shot peening treatments is capable of achieving an optimal surface layer. In Peryer [23] another paper, after laser shock peening process, fatigue tests carried out no notched samples displayed about 30% maximum increases of the fatigue limits.

Advantage of the Laser Shot Peening

The potential benefits of the laser technique are to induce the surface of components residual compressive stress to a magnitude equivalent to that achieved by conventional shot peeing, which is approximately 60% of the ultimate tensile stress of the material. Components most likely to benefit from the technique are in the aerospace industry and especially aero engine components such as blades, discs and rotors, but application are also possible in the automotive, medical, petrochemical and power generation industries.

The most application of laser shot peening is in the aero engine part such as compressor and turbine blades, which may be damaged by the ingested foreign objects. It can be used to achieve the satisfactory result without change the surface which can be a critical factor effects the fuel efficiency and balance. Further, the precise depth of residual stress can be controlled by applying successive shocks to the small area. This derives the residual stress progressively deeper without exceeding the

limited of the material at the surface. The extensions of service life can be somewhere from 310 times the extension compared to the normal shot peening. The main reason is that laser peening puts compressive stress much deeper into the part.

However, it should be noted that when the shot peening introduced, it is possible to damage the surface by excessive peening or rolling if it is conventional shot peening. Experience and testing are required to establish the proper conditions which produce the optimum residual stress distribution. [24]

3.5 **Low Plasticity Burnishing**

The concept of low plasticity burnishing (LPB) originated at Lambda research, as a means of producing a layer of compressive residual stress of high magnitude and depth with minimal cold work, LPB can be performed with conventional CNC machine tools allowing parts to be processed during manufacturing rather than as a post process in a separate facility.

The process is characterized by the use of a single point contact achieved with a smooth free rolling spherical ball, the ball is supported in a fluid bearing under sufficiently high pressure to lift the ball to the surface of the retaining spherical socket. The ball is in mechanical contact only with the surface to be burnished.

Controlling the path of the tool in a CNC lathe or milling machines, allows the tool to deform any point ensuring that the depth of compressive stress from any surface penetrated no greater than 10 % of the section thickness. It is measured by X-ray method.

Considering the low plasticity burnishing, it can be accomplished with conventional CNC machine tools. It can reach a maximum beneath the surface. When using shot peening, because each shot impacts the surface at a random location and it results in many multiple impacts, producing a highly

cold worded surface layer. While applying laser shot peening, the cold work is accumulative, multiple laser shot peening shock cycles may produce an accumulation of the cold work. Laser shot peening achieves maximum compression with minimum cold working. The best part is cheaper than laser shock peening process. From practice point of view, when the job of improving some specimens is proceeded, the technology is considered. At the mean time, the cost and other factors are needed to access in all process.

Lastly, I proposes that the applicability of using the high velocity water shot when forming the surface residual stress, which can avoid the machine cost and consequent effect such as surface roughness. The difficult portion of experiment is to control the pressure in the volume, velocity and distribution in the form of uniformities.

Conclusions

The induced beneficial compressive residual stress to the specimen via methods such as autogrettage, cold expansion, shot peening, laser shock peening and low plasticity burnishing are discussed in detailed and all shows the improvement to the fatigue life.

Chapter 3 Residual Stress Evaluation Methods

Over the last few decades, various quantities and qualitative methods have been developed. In general, a distinction is made between destructive and non-destructive techniques.

The first series of methods is based on destruction of the state of equilibrium of the residual stress after sectioning of the mechanical component, machining or layer removal. The redistribution of the internal forces leads to local strains, which are measured to evaluate the residual stress field. The residual stress is deduced from the measured strain using the elastic theory (analytical approach or finite element calculations).

These techniques are only sensitive to the macroscopic residual stress. The most usual methods are:

- The hole drilling method,
- The ring core technique,
- Layer removal method
- The sectioning method.

The second series of methods is based on the relationship between the physical and crystallographic parameters and the residual stress. The most developed methods are:

- The X-ray and neutron diffraction method.
- The ultrasonic techniques.
- The magnetic methods
- Raman Spectroscopy
- Synchrotrons

3.1 Hole Drilling Method

3.1.1 Background

Stresses will be relaxed when introducing a hole in a stressed body. The relaxation which occurs can be monitored through a specifically designed strain gage rosette. The hole is drilled in the center of the strain gage grids. The average residual stress occurring over the depth of the drilled hole can be calculated from the strain relaxations.

The hole-drilling method (ASTM Standard E837) relies on stress relaxation when a hole is drilled into the centre of a rosette strain gage when the strain gage is used as in determining the strain. When the material is removed by drilling, the extent of the strain relief is monitored by the strain gages or other strain measurement methods and the direction and magnitude of the principal stresses can be calculated.

A special high-speed air turbine drill, as shown in below Figure 3-1, is used to first locate the drill to within 0.001inch of the rosette centre and then to remove material to a controlled depth. At each depth increment, the strain relief on each of the gages is measured and converted into stress. As subsequent material removals occur, the stress distribution as a function of depth can be determined.

Figure 3-1 High-speed air turbine drill

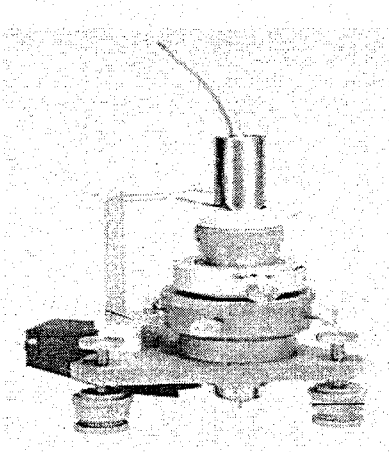

The important consideration in the method is the ability to drill the relief hole so as not to introduce new stresses. This is best achieved in hard materials by use of a high-speed turbine drill which avoids excessive rubbing of the cutting surface against the hole wall. As a result of careful design of the tool, the holes have flat bottoms and straight walls as required by ASTM E837.

The accuracy of the hole-drilling method is directly related to the ability of locating the hole accurately in the centre of the rosette. As an example, if the hole is no more than 0.001" off centre, the residual strain error is less than 3%. In practice, the location accuracy is better than this, so the overall accuracy in residual stress measurements is quite good.

Based on the limitation of the strain gage method, the Digital Speckle Correlation method has the obvious advantage over the strain gage because no matter where the hole is drilled, the subset of whole image can be moved respectively until the best location can be located. The a ignment of the centre of drilled hole and the strain gages centre will be not be obstacle any more in the experiment.

Feature of Hole Drilling Method

- An established method standardized by ASTM Procedure E837.
- Customized strain gages.
- Method only valid for residual stresses up to nominally 50% of yield strength.
- Highly sensitive to position and shape of drilled hole.
- Residual stresses determined are the average over the depth of drilled hole.
- Incremental technique offers qualitative results only

Application of Hole Drilling Method

- Austenitic stainless steel weldments.
- Cast iron piping.
- Forged nickel base alloy disk components.
- Welded titanium pipes.

- Dual phase stainless steel rollers.
- Inertia welded jet-engine disks.

Mathar[25] first proposed that every perpendicular to a free surface is necessarily a principal axis on which the shear and normal stresses are zero. The elimination of these stresses on the hole surface changes the stress in the immediately surrounding region, causing the local strains on the surface of the test object to change correspondingly.

3.1.2 Through Hole Analysis

Through hole drilling is based on the basis of a small hole drilled completely through a thin, wide, flat plate subjected to uniform plane stress. A local area within a thin plate which is subject to a uniform residual stress. Set up the stain gages and drilling a through hole in the geometry center of the rosette and obtained the relaxed the strains.

Subtracting the initial stresses from the final (after drilling) stresses gives the change in stress at point $P\ (R\ ,\ \alpha\ )$ due to drilling the hole.

If the material of the plate is homogeneous and isotropic in its mechanical properties, and linear-elastic in its stress/strain behaviour, by using biaxial Hooke's law to solve for the relieved normal strains at the point $P(R\ ,\ \alpha\ )$. The resulting expressions are as follows:

$$\varepsilon_r = -\frac{\sigma_x(1+\nu)}{2E}\left[\frac{1}{r^2} - \frac{3}{r^4}\cos 2\alpha + \frac{4}{r^2(1+\nu)}\cos 2\alpha\right] \qquad 3.1$$

$$\varepsilon_\theta = -\frac{\sigma_x(1+\nu)}{2E}\left[-\frac{1}{r^2} + \frac{3}{r^4}\cos 2\alpha - \frac{4\nu}{r^2(1+\nu)}\cos 2\alpha\right] \qquad 3.2$$

They can be written in a simpler form, demonstrating that along a circle at any radius $R\ (R \geq R_o)$ the relieved radial and tangential strains vary in a sinusoidal manner:

$$\varepsilon_r = \sigma_x (A + B\cos 2\alpha) \tag{3.3}$$

$$\varepsilon_\theta = \sigma_x (-A + C\cos 2\alpha) \tag{3.4}$$

while A, B and C stand for:

$$A = -\frac{1+\nu}{2E}\left(\frac{1}{r^2}\right)$$

$$B = -\frac{1+\nu}{2E}\left[\left(\frac{4}{1+\nu}\right)\frac{1}{r^2} - \frac{3}{r^4}\right]$$

$$C = -\frac{1+\nu}{2E}\left[-\left(\frac{4\nu}{1+\nu}\right)\frac{1}{r^2} + \frac{3}{r^4}\right]$$

In practice, residual stresses are more often biaxial rather than the above mentioned unaixal condition. The following equations establish the relationship between the released strain and principal stresses and their direction.

$$\sigma_{max} = \frac{\varepsilon_1 + \varepsilon_3}{4A} - \frac{1}{4B}\sqrt{(\varepsilon_3 - \varepsilon_1)^2 + (\varepsilon_3 + \varepsilon_1 - 2\varepsilon_2)^2} \tag{3.5}$$

$$\sigma_{min} = \frac{\varepsilon_1 + \varepsilon_3}{4A} + \frac{1}{4B}\sqrt{(\varepsilon_3 - \varepsilon_1)^2 + (\varepsilon_3 + \varepsilon_1 - 2\varepsilon_2)^2} \tag{3.6}$$

$$\tan 2\alpha = \frac{\varepsilon_1 - 2\varepsilon_2 + \varepsilon_3}{\varepsilon_1 - \varepsilon_3} \tag{3.7}$$

where ε_1, ε_2 and ε_3 are the measured value of the strain gages, A and B are coefficients, σ_{max} and σ_{min} are the principle stresses, α is principle direction.

Determining Coefficients $\overline{A}$ and $\overline{B}$

The advantage of experimental calibration is that it is potentially the most accurate means for determining the coefficients when performed correctly with sufficient attention to detail. And its disadvantage is that it must be repeated each time a different set of geometric parameters involved. The steps in the calibration procedure can be as follows:

1. Zero-balance the strain gage circuits;
2. Apply a load, P, to the specimen to develop the desired calibration stress, σ_c.
3. Measure strains ε_1' and ε_3' (before drilling);
4. Unload the specimen, and remove it from the testing machine;
5. Drill the hole;
6. Replace the specimen in the testing machine, re-zero the strain gage circuits, and then reapply exactly the same load, P.
7. Measure strains ε''_1 and ε''_3 (after drilling).

The calibration strains or the relaxed strains corresponding to the load, P, and the stress, σ_c, are then:

$$\varepsilon_{c1} = \varepsilon_1'' - \varepsilon_1' \qquad 3.8$$

$$\varepsilon_{c3} = \varepsilon_3'' - \varepsilon_3' \qquad 3.9$$

$$\varepsilon_{c1} = \sigma_c\left[\overline{A} + \overline{B}\cos\left(0^\circ\right)\right] = \sigma_c\left(\overline{A} + \overline{B}\right)$$

$$\varepsilon_{c3} = \sigma_c\left[\overline{A} + \overline{B}\cos\left(2\times 90^\circ\right)\right] = \sigma_c\left(\overline{A} - \overline{B}\right) \qquad 3.10 \text{ \& } 3.11$$

Solving for $\bar{A}$ and $\bar{B}$,

$$\bar{A} = \frac{\varepsilon_{c1} + \varepsilon_{c3}}{2\sigma_c}$$

$$\bar{B} = \frac{\varepsilon_{c1} - \varepsilon_{c3}}{2\sigma_c}$$

3.1.3 Blind-Hole Analysis

As we discussed above, the through hole drilling configuration is not typical of practical test objects. The practical specimens can be of any size or shape, and are rarely thin or flat. Because of this, a shallow "blind" hole is used in most applications of the hole-drilling method. Due to introducing a very complex local stress state by drilling a blind hole, there is not close form by the theory of elasticity.

Rendler and Vigness [26] showed that Blind hole closely parallels the through-hole condition in the general nature of the stress distribution. The relieved strains due to drilling the blind hole still vary sinusoidally along a circle concentric with the hole in the manner as the through hole if appropriate blind-hole coefficients $\bar{A}$and $\bar{B}$ are employed, which can be obtained by experimental calibration or by numerical procedures such as finite-element analysis.

Now, for any given initial state of residual stress and a fixed hole diameter, the relieved strains generally increase (at a decreasing rate) as the hole depth is increased. Therefore, in order to maximize the strain signals, the hole is normally drilled to a depth corresponding to at least $Z / D = 0.4$

Schajer [27] introduced two new coefficients, denoted here as $\bar{a}$and $\bar{b}$, and defined as follows:

$$\bar{a} = -\frac{2E\bar{A}}{1+\nu} \qquad 3.12$$

$$\bar{b} = -2E\bar{B} \qquad 3.13$$

where coefficients $\bar{A}$and $\bar{B}$ can be obtained from the above section "though hole drilling".

3.1.4 Accuracy and Validation

It is noticed that when drilling a hole, the drilling machining system can be end-mill cutting, air abrasion, electro-chemical and high-speed drilling. They can induce the machining strains. So this kind of machining strain needs to be examined before final calculating the residual stress. The study shows that these stresses are not equal bi-axial or axisymmetric. The induced stress can be determined by the means of performing hole drilling (possibly several times) on a sample of stress-relieved material and collect the induced strains. Average the strains from the three gages at each hole depth and use the averages as the representatives of the induced strains. One of the solutions is to apply a machining technique that induces minimal additional stresses. One study [29] indicated that if the statistical average of the total induced strain registered by each of the strain gages is not greater than 5ue, then the resultant calculations of the residual stresses are acceptable.

Another study has been done and showing the strong evidence that hole drilling may be used reliably to determine the residuals tested in the engineering components which made of the investigated materials by comparing the result obtained by destructive with non-destructive methods.[30]

A Effect of Hole eccentricity

Although caution has been made to ensure the hole is to be drilled in the center of strain gage rosette, the misalign still can contribute to the erroneous calculations to residual stress. Wang [31] established

the relationship between the relieved strains which are obtained from the off-center drilled hole to the "real" center residual stresses. The equation and its schematic as figure 3-2 as follows:

$$\begin{bmatrix} A_1 & B_1 & C_1 \\ A_2 & B_2 & C_2 \\ A_3 & B_3 & C_3 \end{bmatrix} \begin{pmatrix} \sigma_1 + \sigma_2 \\ (\sigma_1 - \sigma_2)COS2\theta \\ (\sigma_1 - \sigma_2)SIN2\theta \end{pmatrix} = \begin{pmatrix} \varepsilon_1 \\ \varepsilon_2 \\ \varepsilon_3 \end{pmatrix}$$

Where

$$A_i = -\frac{1}{2E}(1+\upsilon) r_i^2 \cos 2\alpha_i \qquad 3.14$$

$$B_i = -\frac{1}{E}[(1-\upsilon) r_i^2 \cos 2\alpha_i + (1+\upsilon) r_i^2 (1 - \frac{3}{2} r_i^2) \cos 2(\theta_i - \alpha_i)]$$

$$C_i = -\frac{1}{E}[(1-\upsilon) r_i^2 \sin 2\alpha_i + (1+\upsilon) r_i^2 (1 - \frac{3}{2} r_i^2) \sin 2(\theta_i - \alpha_i)]$$

$r_i = r / R_i$ where r is the hole radius normalized with respect to the distance from o' to the center of the gage i;

θ_i and α_i are the orientation and offset angles of the gage i respectively;

o is the rosettes center;

R is the distance form the rosette center to the gage center;

β and e are the eccentricity and the offset angle of the hole center o' with respect to the point o;

ξ_i is the orientation of gage i with respect to the system of coordinates XOY.

Figure 3-2 Schematic of Measurement

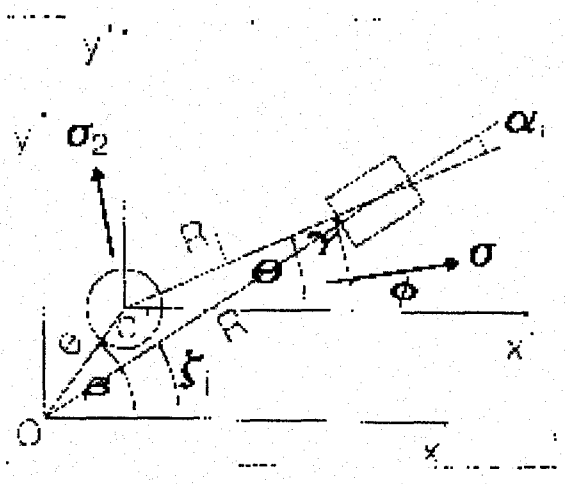

From the Sasaki [32] by comparing the simulated residual stress with the actual residual stress and concluded that when a hole is drilled without eccentricity, the residual stressed can be estimated within 3 percent of error at most by the five gage method and 5 percent of error at most by the three gage method. Also, the accuracy of residual stress measurement increases with decreasing distance of strain gage, r/R. Even when the hole is drilled eccentrically and when the hole is close to the boundary, the residual stresses can be estimated within 20 to 30 percent of error by the three gages.

B Effect of Stress Gradients

If the stresses vary below the material surface, the accuracy of their determination depends on the increments of the hole drilling. It is difficult to predict the pattern of stress distribution in the majority of engineering problems. In ASTM [33] test, the stress gradients may be determined with reasonable accuracy, if the increments are approximately 0.12 mm. As to the steep gradient, the smaller the increment is achieved, the better the accuracy can get. In doing so, the accuracy of the instrument has been to be ensured in order to meet the requirement.

C Effect of Plasticity Deformation

If hole drilling is performed in a specimen in which the residual stress state is uniaxial or equal bi-axial and greater than 1/3 or 0/5 σ_y some region around the hole's perimeter will be plastically deformed, which violates the basic assumption of laws of linear elasticity. There are two solutions available so far to improve the analysis for the cases of high stress. Lu [34] proposed a gage layout that consists of sequences of gages along the three major directions.

Li. and Liu [35] proposed another approach by estimating the state of plastic deformation at the hole region that results from stress concentration. Strains before and after hole drilling under these loads would have be recorded, and calibration curves charted. From these data, the appropriate formulas that relate the measured strains and the measured stress would be developed.

D Effect of Experimental techniques

In this section, the techniques such as drilling system, surface preparation and choice of strain gage has been discussed due to their effort to the experiment measurement. Serious consideration can ensure the precise measurement and satisfactory result.

Drilling system

In the following Table 3-1, the comparison has been made to the five different drilling tools. The author proposes laser in drilling the hole. The advantage can control easily the increment and assure the drilled-hole center aligning the rosette center and the bottom. However, it should be noted that the diameter cannot be too large. And due to the size of the hole can be very small, the relaxed strain has be detected by more sensitivity instruments.

Conclusion

Abrasive jet system, High-speed turbine system and Milling machine are strongly recommended to measure the residual stress. Abrasive jet system is the standard method for verifying the other technique where a danger of introducing machining residual stress.

Table 3-1 Comparing Five Different Drilling Tools

Name	Advantage	Disadvantage	Stress free	Portability
Classical drilling system	Done easily, can be hard materials	Low-speed end mill induced large proportion of stress	N/A	N/A
Electrical discharge machining system	Conducting materials	Surface integrity affected by the heating; protecting the strain gage	N/A	N/A
Abrasive jet system		No flat bottom, not for incremental drilling	Yes	Yes
High-speed turbine system	Portable; can be center and incremental, flat bottom	Not for hard material not for big diameter.	Yes	Yes
Milling machine	Can be big hole and for ceramic coating; stable.		Yes	Yes

To be noted, as to the bulk ceramic material, a diamond drill can be used to achieve the drilling.

2) Surface preparation of the sample

The normal way to preparing the surface is using the abrasive paper or other mechanical technique which can generate considerable amount of residual stress to the object. It should be kept in the minimal. The solution is just to keep it when measuring or polish the surface by X-ray diffraction method.

3) Choice of strain gage

Here in Table 3-2 list some gages which are commonly used.

Table 3-2 List of Stain Gage

MMRE031, MM-R 3062, 125, HBM RY61 RY21, TNK I RS2, TML FRS3	Depth less than 4 mm, 3 gage rosette
MM- XX-062	Edge of weld bead
TML-F A-05-8R	8-gage rosette

The strain gage shown i the table can be referred from reference 1.

3.1.5 Properties, factors and techniques issues

A Residual stress measurement in Orthotropic material

There are many materials such as fiber-reinforced composites has anisotropic elastic properties, which cannot be applied by the same approach.. Schajer and Yang [36] presented a different solution method can be used for materials of any degree of elastic orthotropic. For an isotropic material, the relived strain measured by a strain gage whose axial is inclined at an angle θ from the x direction is:

$$\varepsilon_r = A(\sigma_x + \sigma_y) + B(\sigma_x - \sigma_y)\cos 2\theta + C\tau_{xy}\sin 2\theta \qquad 3.15$$

The above equation can be rewritten in matrix form to relate the three measured strains $\varepsilon_1, \varepsilon_2, \varepsilon_3$ to the Cartesian stress. In the orthotropic case, the above equation can be generalized to

$$\begin{bmatrix} A+B & 0 & A-B \\ A & -C & A \\ A-B & 0 & A+B \end{bmatrix} \begin{bmatrix} \sigma_X \\ \tau_{XY} \\ \sigma_Y \end{bmatrix} = \begin{bmatrix} \varepsilon_1 \\ \varepsilon_2 \\ \varepsilon_3 \end{bmatrix} \qquad 3.16$$

Where the elastic compliances are depending on the orthotropic elastic properties of the specimen, the hole diameter and the strain-gage rosette geometry.

And the list of numerical values of the compliance values to be used in the above equation for a range of elastic constants has been determined on the paper. Consequently the experiments have been carried out in verifying the method. The result is quite agreeable between the expected and the measured values. One of the error sources is the variation in the material properties of the test specimens.

B Modified hole-drilling technique

In the conventional procedure, the amount of relaxation for a given strain-gage hole configuration, material and drilling procedure is measured for a known stress distribution. From the measured values, relaxation coefficients are calculated and used to determine residual stresses, using identical test conditions, in an unknown stress fieled. Am, Nawwar and J, Shewchuk[37] proposed a new technique by which can remove the necessity for calibration of each experimental setup. The relaxation coefficients are calculated from theory and the strain components which are extraneous to the true relation strain are separated from the measured value.

The net relaxation strain is used to calculate the residual stress at the point of measurement

$$\sigma_x = \varepsilon_R \cdot \frac{E}{K_r(\lambda,\theta)} \qquad 3.17$$

Where $K_r(\lambda,\theta) = -\{\frac{(\upsilon+1)}{8}\lambda^2 + [\frac{1}{2}\lambda^2 - \frac{3(\upsilon+1)}{32}\lambda^4]\cos 2\theta\}$

λ is the radial relaxation coefficient, Is the no dimensional hole diameter which is the ration of the hole size.

d to the center distance between the hole and strain gage

θ the angular orientation of the strain gage

And this technique can extend the range of measurements to thin plates as well as thick plates.

In the experiment section, the researcher performed the outward-drilling sequence which is found correction for stress redistribution. The experiment showed that the change of stress at any loca ion is proportional to the residual stress. So it is reasonable to assume that a similar reduction of stress at the location of drilling has taken place during the action of drilling. This will, in turn, result in an error in estimating the residual stress at the location of drilling.

The conclusion is drawn that the technique may be used to measure residual stress distribution. Its accuracy is affected by the observed redistribution of residual stresses due to drilling and the interaction between holes.

C A new Rosette design in improving the reliability

Schajer and Tootoonian [38] proposed a new Rosette design for more reliable hole drilling residual stress measurements. The objectives are to increase the overall sensitivity of the strain measurements and to increase the strain sensitivity to interior stresses. In assessing the strain gage direction, after comparing with the traditional gage used in the ASTM which is rectangular gage with parallel grid

line. The gage with the radial and circumferential direction looks more promising.

The three factors of the gage size can be the inner radius, the angular span and the outer radius. The inner radius is chosen to be large enough to accommodate the maximum desired hole size. 30 degree of the angular has been chosen to maximize the thermal stability. Because small outer radius maximizes strain response and calibration constants a and b, so a small value is chosen.

As to the rosette layout, based on the feature of the circumferential rosette can give strains that are opposite in sign to those of the radial gage, the author proposed the combination of the radial and circumferential geometry as follows in Figure 3-3:

Figure 3-3 Newly Designed Rosette

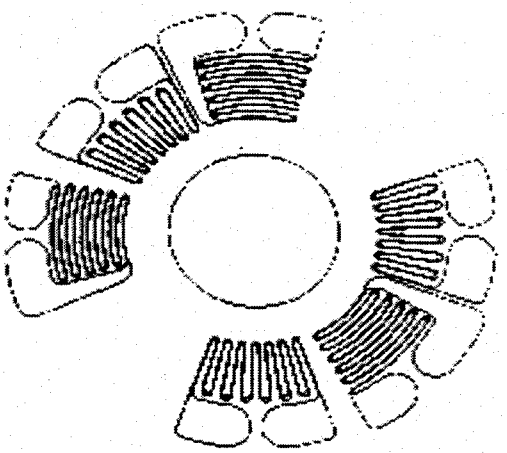

This kind of Rosette layout has the advantage of higher overall stain sensitivity; without localizing the strain measurement close to the hole edge; half bridge circuits greatly reduced extraneous thermal strains and electrical noise.

In the section of experimental measurement, this layout and the ASTM measurement have compared

with the theoretical method. The calibration constants a and b has been improve by 130 % and 60% respectively, which increase residual stress accuracy.

D Induced drilling stressed in the center-hole method

When applying center hole drilling method in determining the residual stress which varies with depth, the semi-empirical procedures have been suggested to overcome this problem by requiring the precise increment by drilling the hole. Therefore, the more precise the increment, the better the result can be achieved. And the flat-bottom is required as well.

Flaman [54] suggested use ultra-high-speed drill (UHS) rather than conventional low-speed (LS) mill. In his experiment, five different specimens have been used by the two methods. The result shows as follows in Table 3-3:

Table 3-3 Magnitude of total average relief stains as measured by the three gages of the strain Rosette on stress-relieved specimens

	Ultra-high-speed drill	Low-speed End mill
Mild steel	-6	-40
Stainless steel	-4	-293
Nickel	+3	-169
Aluminium	-54	-169
Copper	-81	-2843

In addition, firstly the sides of hole in UHS is much smoother and straighter than that of LS; secondly the bottom of the hole made by UHS is much flatter and less rounded than that of LS. The conclusion is made that the ultra-high-speed drill is general much superior to the low-speed end mill with respect to induced machining stressed for use in the center hold method for residual stress measurement.

Discussion

The relieved strains decay quite rapidly with distance from the edge of the hole, the gages only measure about 25-40% of the original residual strains at the hole location. If the relative decay rate can be determined, it is can be used to establish the relationship with the relieved strains, therefore we can obtain the relieved strain without compromising the decaying.

Conclusion

The hold drilling method is very popularly used and well standardized in the ASTM. It has the advantage of less time consuming, less cost and a board range of material applications.

3.2 RING CORE (TREPAN) METHOD

The ring-core method[1] is a mechanical/strain gage technique employed to describe the principal residual stress field as a function of depth in polycrystalline or amorphous materials. The method involves placing a strain gage rosette at the surface at the location of interest on a give component. An annular groove is machined around the strain gage rosette at predetermined depth increments. The strain relaxation which occurs as a function of machined depth is recorded. The entire process and data collection are controlled by an on-line computer. The final residual stress values are calculated using the measured change in strain with depth.

The ring-core method is generally used when x-ray diffraction residual stress measurements are not feasible. The ring-core method works well on materials which are of coarse grained, such as cast metals or weldments. The ring-core technique can be used on ceramics and plastics as well as metallic materials.

Feature of Ring-core Method

- Principal residual stresses are determined as a function of depth.
- Method valid for residual stresses up to 100% of yield strength.
- Low sensitivity to placement of strain gage and eccentricity of the machined ring.
- Low sensitivity near the surface.

Two methods employed at Lambda Research, the ring-core or trepanning method and the center-hole drilling method, allow the residual stresses to be determined mechanically by the relaxation of strains in arbitrary geometries and stress fields. Both methods have been used extensively for residual stress measurement in coarse grained or even amorphous materials. Orthotropic solutions and software have been developed at Lambda Research using the method of Schajer and Yang [40] for composite materials.

Lambda Research p ovides residual stress determination in alloys, ceramics and composites through mechanical methods These techniques are utilized when x-ray diffraction methods are not feasible, such as for coarse gr ned castings or weldments which do not have an adequate amount of diffracting grains. The mechanic l methods are also used to determine the residual stress in materials which do not have a useable diffraction peak for x-ray residual stress evaluation or when integration over larger volumes is desirable.

A variety of geometry and stress field dependent mechanical methods have been developed, such as Sachs' method for boring or Letner's layer removal procedures. Such mechanical techniques are applicable only to specific, simple specimen geometries and symmetrical stress fields, the varity of application is limited.

3.3 Layer removal method

The principle of this r ethod is a plane part which contains residual stresses is deformed in such a way

as to maintain the static equilibrium of the internal moment and forces. On a thin parallelepipedal test specimen, this deformation is represented by the deflection(f). The deflection naturally depends on the type and magnitude of the residual stressed involved, whose distribution throughout the thickness of the material can be characterized by a function $\sigma_e(e)$, where e is the thickness of the layer being considered with respect to the surface area of the part.

If the layers of material in which there are residual stresses which are gradually removed by chemical machining, the balance of internal stresses and moments is upset at the same time. To re-establish this balance, the part has to change shape. The variation in deflection (df) produced by removing a layer of thickness (de) can be related to the surface stress $\sigma_e(e)$ which existed in the removed layer by equation:

$$\sigma_e(e) = -\frac{4}{3}E\frac{e^2}{l^2} * \frac{df}{de} \qquad 3.18$$

Where 1 represents the length on which the deflection is measured and E is the Young's modulus of the materials.

This equation is based on the following hypotheses:

1) The pre-stressed test specimen is homogeneous and isotropic; its axes coincide with those of the principal stresses
2) The stress in the direction of the thickness is negligible.
3) The transverse stresses will initially be considered negligible although, strictly speaking, they should be taken into account.

Therefore, only the principal stress $\sigma_e(e)$ parallel to the axis of the test specimens will be considered. It will be likened to a girder subjected to a constant bending moment, which therefore has a constant

curve. The stress will only vary according to the depth and will be identical along the entire length and width of the test specimen.

3.4 The Sectioning Method

The principle[1] is that when stress is induced in a body without the action of external load, the stress is called residual stress which is self-equilibrating, and the source of residual stress should exist in the body.

The source of residual stress is incompatible strain which is called here "inherent strain." As an example, when a stress free body is subjected to temperature change locally. Thermal stress is produced in the body, the thermal strain due to temperature change is regarded as inherent strain. In the case of welded joints, the source of residual stress is plastic strain including dislocation. The inherent strain is generally produced as the result of thermal elastic-plastic behavior.

When the object is cut without producing new plastic strain for measurement of residual stress, the magnitude and distribution of the inherent strain do not change, but the stress distribution changes due to relief of stress which as acting on the newly exposed surfaced before cutting.

Paying attention to three-dimensional residual stress, one approach is the so-called sectioning method, by which the measuring object is sectioned and the stress is relaxed. In order to measure three-dimensional residual stress, the stress distributing which was action on the newly exposed surfaces of the measuring object before sectioning is estimated from relaxed strains observed on the surface during sectioning. The sectioning is applied repeatedly to the sectioned pieces until no relaxation strain is observed. In this procedure, section stress in the sectioned plane is dealt as a parameter for measurement.

3.5 X-Ray Method

X-Ray Diffraction is a common non-destructive technique that can be used to determine the levels of residual stress in a component. X-rays probe a very thin surface layer of material (typically tens of microns). Through knowledge of the wavelength, the change in the Bragg angle, and the changes in interplanar spacing, the elastic strain may be calculated

The $sin^2\ \Psi$ method is a sensitive and accurate technique to measure residual stresses in a fine-grained, polycrystalline material.

As shown in Figure 3-4 shown below, the position of a diffraction peak will shift as the sample is rotated by an angle Ψ. The magnitude of the shift will be related to the magnitude of the residual stress.

Shift of diffraction peak with change in Ψ value. Note that as Ψ increases in b) and c) that above the position of the diffraction peak the shift further away from its usual position in a). Thus, if there is no residual stress, the shift will be zero. The relationship between the peak shift and the residual stress σ is given by

$$\sigma = \frac{E}{(1+\nu)\sin^2\Psi}\,\frac{(d_n - d_0)}{d_0} \qquad 3.19$$

where E is Young's modulus, v is Poisson's ratio, Ψ is the tilt angle, and d_i are the "d" spacings measured at each tilt angle. If there are no shear strains present in the sample, the "d" spacings would change linearly with $sin^2\ \Psi$ and a least-squares fit to the curve (for multiple values of Ψ) would give σ. However, if shear strains are present, a splitting of the plot will occur and the analysis is more complicated. Finally, if the sample is rotated in-plane, it is possible to determine the principal stresses and their directions.

Figure 3-4 Schematic of X-ray Method

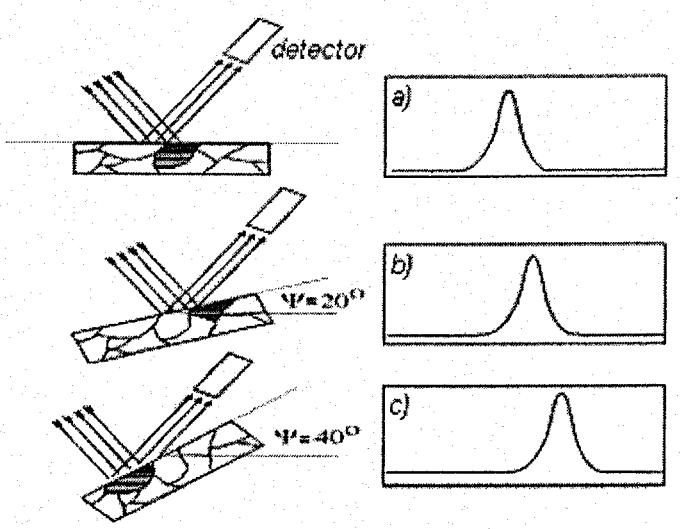

3.6 The Neutron Diffraction Method

The principle of neutron diffraction method, the components of strain are obtained from measurements of change Δd in the lattice spacing d of crystals. When a beam of neutrons of fixed wavelength λ is incident upon a crystalline specimen, a diffraction pattern with sharp maximum is produced, the positions of the peaks are given by the Bragg equation $2d\sin\theta = n\lambda$ Where n is an integer and 2θ the diffraction angle. A small change in the lattice parameter Δd will result in a change $\Delta\theta$ in the Bragg angle so that the lattice elastic strain in the direction of the scattering vector Q is given by[41]

$$\varepsilon = \frac{\Delta d}{d} = -\Delta\cot\theta \qquad 3.20$$

Only the neutron diffraction method is capable of making satisfactory residual stress measurements non-destructively within the interior of materials. Like other diffraction techniques, neutron diffraction relies on elastic deformations within a polycrystalline material that cause changes in the spacing of the lattice planes from their stress free value. Measurements are carried out in much the

same way as with X-Ray diffraction, with a detector moving around the sample, locating the positions of high intensity diffracted beams.

The difference between the X-ray diffraction and neutron diffraction method is made. There are many situations where X-ray diffraction is not useful for measuring residual stresses. These include non-crystalline materials, large-grained materials, nano-materials, textured, or heavily deformed metals. While in these cases, the neutron can success applied.

The greatest advantage that neutrons have over X-Rays is the very large penetration depths, which makes them capable of measuring at near surface depths of around 0.2mm down to bulk measurements of up to 250mm in aluminum or 37mm in steel. Therefore, this advantage of neutron diffraction method will play an important role in measuring the near surface depth residual stress which induced by the autofrettage and shot peening.

Another advantage of neutron diffraction can provide complete three-dimensional strain maps of engineered components. This is achieved through translational and rotational movements about the center axis of the test piece.

This method of stress evaluation, with its capacity to collect large quantities of accurate data (via position sensitive detectors) over the whole surface and depth (depending on the thickness of the sample), has made neutron diffraction a particularly useful techniques.

3.7 The Ultrasonic Techniques

Ultrasonic methods utilize the sensitivities of the velocity of ultrasound waves traveling through a solid to the stress levels within it.[1] Changes in the speed of ultrasonic waves in a material are directly affected by the magnitude and direction of stresses present. Because the velocity changes are

small and are sensitive to the material's texture (grain alignment) it is often more practical to measure transit times as the ultrasonic path length is usually not known to sufficiently high precision. Because the changes in velocity depend on the stress field over the entire ultrasonic path, the spatial resolution is poor. The acoustoelastic coefficients necessary for the analyses are usually calculated from calibration tests.

Whilst ultrasonic methods provide a measure of the macro residual stresses over a large volume of material, the presence of texture in the material often restricts their spatial resolution. Nevertheless, they have the advantage of being able to measure in the bulk of the material and are therefore well suited to routine inspection operations. Additionally, the instrumentation is portable and quick to implement.

3.8 Magnetic Methods

The ferromagnetic properties of steels and other ferromagnetic materials are sensitive to the internal stress state due to magnetostriction and the consequent magnetoelastic effect.[1] Magnetostriction is the process whereby each magnetic domain is strained along its direction of magnetization. At minimum energy the magnetisation will align with the crystalline directions - the magnetic easy axes. A change in the stress level will result in a change in the number of domains aligned along each of the easy axes leading to a reduction in the magneto elastic energy. Although the stress dependence of the magnetic parameters is quite strong, there are many other variable, such as hardness, texture, grain size, etc. which also affect the measurement. For this reason, a combination of magnetic techniques is required so that the effect of these other variables can be eliminated.

The primary advantages of the magnetic methods are that they are very rapid (measurements normally made in seconds), the equipment is fully portable and can measure biaxial stresses, typically to a depth of ~6-10mm. The weakness of the magnetic techniques is the limited range of materials which can be

examined and the inherent sensitivity to a variety of other micro-structural features.

3.9 Raman Spectroscopy

The Raman effect involves the interaction of light with matter.[1] Incident laser light causes the bonds between atoms to vibrate. Analysis of the scattered light, known as Raman spectrum, reveals vital information about a sample's physical state and chemical structure. This technique is non-destructive and non-invasive and has a high spatial resolution (1 μm or less).

Raman or fluorescence lines shift linearly with variations in hydrostatic stress. This method has fine spatial resolution and by using optical microscopy it is possible to select regions of interest just a few microns in size. The method is essentially a surface strain measurement technique, but with optically transparent materials such as sapphire it is even possible to obtain sub-surface information. Materials that give Raman spectra include silicon carbide and alumina-zirconia ceramics and the method is particularly useful for studying fiber composites.

3.10 Synchrotrons

Synchrotrons, or Hard X-Rays, provide very intense beams of high energy X-Rays.[1] These X-Rays have a much higher depth penetration than conventional X-Rays, around 1-2mm in many materials. This increased penetration depth means that synchrotron diffraction is capable of providing high spatial resolution, three-dimensional maps of strain to millimeter depths in engineered components. This increased penetration depth is one of the major advantages of synchrotron diffraction over conventional X-Ray diffraction.

Another great advantage of synchrotrons is the intense narrow beam size (1mm-10mm). This leads to spatial resolutions that are limited not by the instrument but by the crystallite size within the sample.

The measurement is also very much quicker than with conventional X-Ray diffraction. With measurements times of a fraction of a second detailed strain maps of components can be constructed using a few hours of beam time.

3.10 Conclusion

Due to the characteristics of the above-mentioned measurement methods, they can be applied in the different fields. Therefore, the distinction and the downside and upside should be made clearly before using them. To be note, the cost and measuring requirement are to be considered in the event of selecting the approach.

Chapter 4 Digital Speckle Correlation Method

4.1 Theory

Digital Speckle Correlation is one of the computerized method in finding the displacement, strains and consequently calculate the stress. [42] It produces the displacement (U and V) and their gradients (du/dx, du/dy,dv/dx, dv/dy) by using the Newton-Raphson method of Partial Differential Correlation (shorten as NR method).

4.2 Hard Ware and software requirement

Charge Coupled Device (CCD) camera

Image grabbing board OC300

Pneumatic vibration isolation table

IBM PC

Additional monitor to display images

Fibber optic illumination system by D.O Industry

Specimen and appropriate loading device

4.3 Operation sequence and procedure of DSC

The procedure of DSC can be classified in the following three steps[43]:

Step I To collect or grab all the images and any corresponding initial data needed of the object under load.

Step II To take these two images and data colleted from the PRESP and proceeds to process them

through the techniques in the published paper.

Step III To graphically plot the collected resultant displacement and gradient data.

Basic theory of Digital Speckle Correlation is by using a standard video camera attached to a video digitizer, which transforms the image to a 512X512 set of numbers representing the image. Each number represents the intensity of light impinging on the small area of the camera sensor, which is referred to as pixels. Each point is distinguished by its level of darkness and is given by 0-255 numbers, which is called the greyscale. The number of greyscale means total dark (black), and 255 means total bright (white). The value of each pixel is typically an eight-bit number with the lowest value representing black, highest value white and values in between representing different shades of grey.

To compare two digital images so as to determine the deformation between the two images, it becomes a job of comparing subsets of numbers between the two digital images. The correlation is to measure how well (co-ordinates)subsets match; to determine the value for six parameter U, V du/dx, du/dy,dv/dx, dv/dy so as to minimize the correlation coefficient (S).

With the technique, Newton-Raphson method quickly gives corrections or modifications for the initial guess of the six deformation parameters and will converge to the solution with substantially fewer calculations.

At a selected point, a subset F of user set size of M x N (maximum is 101X101 pixel)from the first image is chosen to be compared to a subset G from the second image starting at the same (I, J) location. The subset G (maximum 131X131 pixels) can be selected immediately after selecting the subset F. The schematic is shown in Figure 4-1 as follows:

Figure 4-1 Schematic of DSC subset Comparison

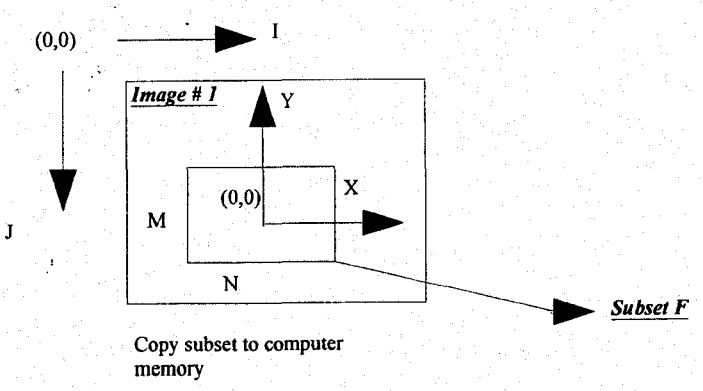

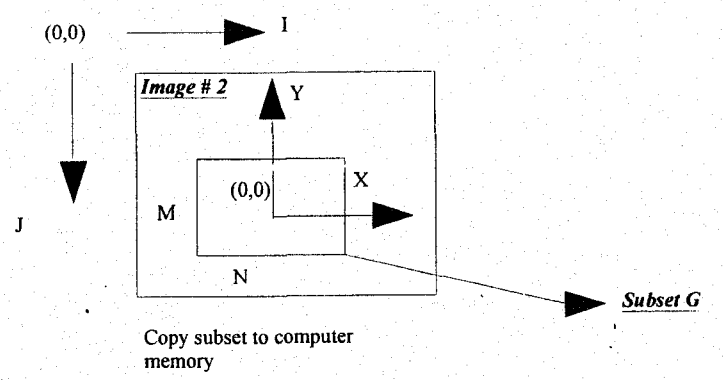

The pixels from both entire subsets are compared and summed in order to calculate the correlation factor S from both entire subset.

$$S(x,y,u,v,\frac{\partial u}{\partial x},\frac{\partial u}{\partial y},\frac{\partial v}{\partial x},\frac{\partial v}{\partial y}) = 1 - \frac{\sum[F(x,y)*G(x^*,y^*)]}{[\sum(F(x,y)^2)*\sum(G(x^*,y^*)^2)]^{1/2}} \quad 4.1$$

where F(x,y) represents the greyscale values of the pixels at the (x, y) and G(x*,y*) represents the greyscale of the pixel at (x*,y*) for the G subsets respectively.

As seen in the 'S' function, both F and G subsets work on an (x,y) coordinate system rather than the screen coordinate system (i,j). This (x,y) system covers the subset size only and has a centre coordinate (0,0) at the center of each F and G subsets. Thus the x coordinates cover ± n-1)/2 and y coordinates cover ±(m-1)/2 for a subset of size m x n:

$$x^* = x + u + \frac{\partial u}{\partial x}\Delta x + \frac{\partial u}{\partial y}\Delta y \quad 4.2$$

$$y^* = y + v + \frac{\partial v}{\partial x}\Delta x + \frac{\partial v}{\partial y}\Delta y \quad 4.3$$

The coordinates (x*, y*) are based on the above two equations which are dependatn on teh values fo x, y, U, V and the gradients du/dx, du/dy, dv/dx and dv/dy. Note that noe of these values correspond to values loaded from the PRESP data and that x* and y* can be between pixels.

The x* and y* can be in between pixels, let us say G(x*, y*) is a greyscale between pixels. In order to calculate a greyscale between pixels, in other words, an approximation of grey level values between pixels is neede , 4 existing pixels around (x*,y*) must be found. These four pixels : round the (x*,y*) are then substit ited into the Lagrange equation to calculate the greyscale G(x*,y*).

There are many methods to do this including the Lagrange equation, Bilinear interpolation and Bicubic spine interpolation, which all aim to approximate the grey level of value. For higher accuracy, the Bicubic spine interpolation has been used.

If the correlation factor S is zero, which means the pixel in F subset exactly coincide with those in G subset, hence the solution is exact. This is never possible due to internal and external noises and the error during the execution of program, which means it is not possible to the grabbed second image is exactly the same as the first image. Therefore the Newton Raphson method produces a solution when close to 0 or when the change in 's' is close to 0. (The user can set the tolerances)

4.4 Theory of Newton-Raphson Method

Newton-Raphson method is for calculation of correction terms which to improve the initial guess. The correction for each guess of the location of the F subset in subset G is given by

$$\Delta P_i = -H^{-1}(P_i) * \nabla(P_i) \qquad 4.4$$

Where if P_i is the translation and gradient values indicating the location of the F subset in subset G or the translation and rotation between imagine #1 and image #2

$$P_i = \begin{pmatrix} u \\ v \\ \frac{\partial u}{\partial x} \\ \frac{\partial u}{\partial y} \\ \frac{\partial v}{\partial x} \\ \frac{\partial v}{\partial y} \end{pmatrix} \qquad 4.5$$

Then the Jacobian matrix is made up of the first order derivative of the correlation function 's' with respect to each term in Pi and H(Pi) is the second order derivatives of the correlation function with respect to each term in Pi. However, the error is found in the row 4 and row 5 in the published paper, the correction has been made and shown in this paper.

$$\nabla(P_i) = \begin{pmatrix} \frac{\partial S}{\partial u} \\ \frac{\partial S}{\partial v} \\ \frac{\partial S}{\partial(\frac{\partial u}{\partial x})} \\ \frac{\partial S}{\partial(\frac{\partial u}{\partial y})} \\ \frac{\partial S}{\partial(\frac{\partial v}{\partial x})} \\ \frac{\partial S}{\partial(\frac{\partial v}{\partial y})} \end{pmatrix} \qquad 4.6$$

$$H(P_i) =$$

$$\begin{pmatrix}
\frac{\partial^2 S}{\partial u \partial u}, \frac{\partial^2 S}{\partial u \partial v}, \frac{\partial^2 S}{\partial u \partial (\frac{\partial u}{\partial x})}, \frac{\partial^2 S}{\partial u \partial (\frac{\partial u}{\partial y})}, \frac{\partial^2 S}{\partial u \partial (\frac{\partial v}{\partial x})}, \frac{\partial^2 S}{\partial u \partial (\frac{\partial v}{\partial y})} \\
\frac{\partial^2 S}{\partial v \partial u}, \frac{\partial^2 S}{\partial v \partial u}, \frac{\partial^2 S}{\partial v \partial (\frac{\partial u}{\partial x})}, \frac{\partial^2 S}{\partial v \partial (\frac{\partial u}{\partial y})}, \frac{\partial^2 S}{\partial v \partial (\frac{\partial v}{\partial x})}, \frac{\partial^2 S}{\partial v \partial (\frac{\partial v}{\partial y})} \\
\frac{\partial^2 S}{\partial (\frac{\partial u}{\partial x}) \partial u}, \frac{\partial^2 S}{\partial (\frac{\partial u}{\partial x}) \partial v}, \frac{\partial^2 S}{\partial (\frac{\partial u}{\partial x}) \partial (\frac{\partial u}{\partial x})}, \frac{\partial^2 S}{\partial (\frac{\partial u}{\partial x}) \partial (\frac{\partial v}{\partial y})}, \frac{\partial^2 S}{\partial (\frac{\partial u}{\partial x}) \partial (\frac{\partial v}{\partial x})}, \frac{\partial^2 S}{\partial (\frac{\partial u}{\partial x}) \partial (\frac{\partial v}{\partial y})} \\
\frac{\partial^2 S}{\partial (\frac{\partial u}{\partial y}) \partial u}, \frac{\partial^2 S}{\partial (\frac{\partial u}{\partial y}) \partial v}, \frac{\partial^2 S}{\partial (\frac{\partial u}{\partial y}) \partial (\frac{\partial u}{\partial x})}, \frac{\partial^2 S}{\partial (\frac{\partial u}{\partial y}) \partial (\frac{\partial v}{\partial y})}, \frac{\partial^2 S}{\partial (\frac{\partial u}{\partial y}) \partial (\frac{\partial v}{\partial x})}, \frac{\partial^2 S}{\partial (\frac{\partial u}{\partial y}) \partial (\frac{\partial v}{\partial y})} \\
\frac{\partial^2 S}{\partial (\frac{\partial v}{\partial x}) \partial u}, \frac{\partial^2 S}{\partial (\frac{\partial v}{\partial x}) \partial v}, \frac{\partial^2 S}{\partial (\frac{\partial v}{\partial x}) \partial (\frac{\partial u}{\partial x})}, \frac{\partial^2 S}{\partial (\frac{\partial v}{\partial x}) \partial (\frac{\partial v}{\partial y})}, \frac{\partial^2 S}{\partial (\frac{\partial v}{\partial x}) \partial (\frac{\partial v}{\partial x})}, \frac{\partial^2 S}{\partial (\frac{\partial v}{\partial x}) \partial (\frac{\partial v}{\partial y})} \\
\frac{\partial^2 S}{\partial (\frac{\partial u}{\partial v}) \partial u}, \frac{\partial^2 S}{\partial (\frac{\partial v}{\partial y}) \partial v}, \frac{\partial^2 S}{\partial (\frac{\partial v}{\partial y}) \partial (\frac{\partial u}{\partial x})}, \frac{\partial^2 S}{\partial (\frac{\partial v}{\partial y}) \partial (\frac{\partial v}{\partial y})}, \frac{\partial^2 S}{\partial (\frac{\partial v}{\partial y}) \partial (\frac{\partial v}{\partial x})}, \frac{\partial^2 S}{\partial (\frac{\partial y}{\partial y}) \partial (\frac{\partial v}{\partial y})}
\end{pmatrix} \quad 4.7$$

Once the correction terms are calculated, they are added to their respective U, V and the gradient terms to produce new corrected U, V and gradient values. This iteration of adding the equation to U, V and gradients is repeated until a close enough answer is produced.

4.5 Proposing An Alternative Searching Tool: Genetic Algorithms Method

Genetic Algorithms (GA) [44] is search algorithms based on the mechanics of natural selection and natural genetics. They combine survival of the fittest among string structures with a structured yet randomized information exchange to formal search algorithm with some of the innovative flair of human search.

Traditional optimization and search methods involve direct search methods which seek local optima by hopping on the function and moving in a direction related to the local gradient(hill-climbing or descending) such as Newton-Ralphson method. These methods have strong reasoning because they use calculus as the driving tools. The advantage of using genetic algorithms is that it is more robust in optimizing discontinuous and noise functions which have rapidly changed points.

GA uses statistics as the driving tool to perform optimization and search methods. The rule of thumb governed in GA is that only the best will stay and the worst will die off. The starting point is selected randomly from a population of points not a single point. Unlike the traditional methods which use a lot of derivatives and other derivatives and other auxiliary knowledge to perform searching, GA uses the objective function directly to perform searching. The type of Direct search can save a lot of computation time.

GA exploits this wealth of information by 1) reproducing high-quality notions according to their performance (reproduction); 2) crossing these notions with many other high-performance notions from other strings (crossover); 3) occasionally flip-flopping the genes of each string pair to create more diversity(mutation).

Applications of GA

Betallo [44] used GA to synthesize a multiplayer radar absorbing coating that maximizes absorption of an electromagnetic wave over a desired range of frequencies and incident angles. The optimization parameters were absorber thickness, permittivity and permeability.

Michigan State University is doing or have recently done a number of interesting projects, both in terms of GA fundamental research and in GA/GP applications, including: automated design. It includes research on composite material design and multi-objective design of automotive components

for crashworthiness, weight savings, and other characteristics automated design of mechatronic systems using bond graphs and genetic programming (NSF) parallelization of GA.

4.6 Advantage, Accuracy and Limitation of Digital Speckle Correlation

The advantage of DSC has been classified in the following:

1) It provides a contour map of the strains (both normal and shear strain) of the released stress rather than at a few points measurement such as the strain gage method;

2) It is simple in set-up, real-time basic and quick in obtaining the result;

3) Human judgment and processing time can been reduced by the accuracy and speed of the computer error is eliminated by computer;

4) It can be applied in the complex geometrical shape;

5) It also can be applied in the area to which people cannot be access such as gas filled chambers, extreme high or low temp environment;

6) Shear strain can be obtained

Accuracy of DSC can be analyzed as follow: comparison of the results obtained by the DSC technique with the actual ones it is proved that the technique works accurately with the maximum error of 5 per cent. The error can be divided into two groups: systematic and random. Systematic error can be an error involved in using a 2D method to measure 3-D displacement field of an object.

The discrete spatial resolution of the CCD camera, the interpolation scheme used to obtain the grey level between two pixel, the displacement shape function adopted for the image subset in searching

for the maximum correlation between two images are the error of the technique itself. Since the systematic errors are repetitive in nature they may be compensated by calibration scheme. Random error can be an error such as errors in pixel readouts and they are also called noise. And it has been noted that limitation of DSC is that this method is still a 2-D measurement and is limited in the area of 3-D field.

Conclusion

In this section, theory, set-up and applications of DSC has been introduced and discussed. One of option search method Genetic Algorithm is suggested. Finally, the advantage, accuracy and limitation of DSC are presente l. The overall picture of this technique is presented for the application in the preceding chapters.

Chapter 5 Residual Stress Determination Using Whole Field Strain Measurement

When the material from a residually stressed body is taken away by drilling a hole, the stress fields in that specific area are released or relaxed. This changes the stress fields in the immediate surrounding region. Because the hole' surface is a free surface, all the shear and normal stress, perpendicular to the hole' surface are zero. This causes the local strain on the surface of the test object to change correspondingly.[46]

Assumption is made by the ASTM E837 that "This test method covers the procedure for determining the residual stresses near the surface of isotropic linearly-elastic materials" and "where the stress do not vary significantly with depth and do not exceed one half of the yield strength".

The residual stress σ_1 and σ_2 are specified in the (x, y) Cartesian system, and its equivalent polar system (r,θ). The hole drilling stresses $\sigma_X, \sigma_Y, \tau_{X,Y}$ are specified with the (X,Y) system and its polar equivalent (R,Θ). The original stress σ state is defined by the transformation equations for plane stress. Visually, it is shown in Figure 5-1 as follows:

Hence the biaxial initial stress state of the residual stress (before the drilling of the hole) expressed in (r,θ) system is given by:

Figure 5-1 Schematic of Initial Stress Definition

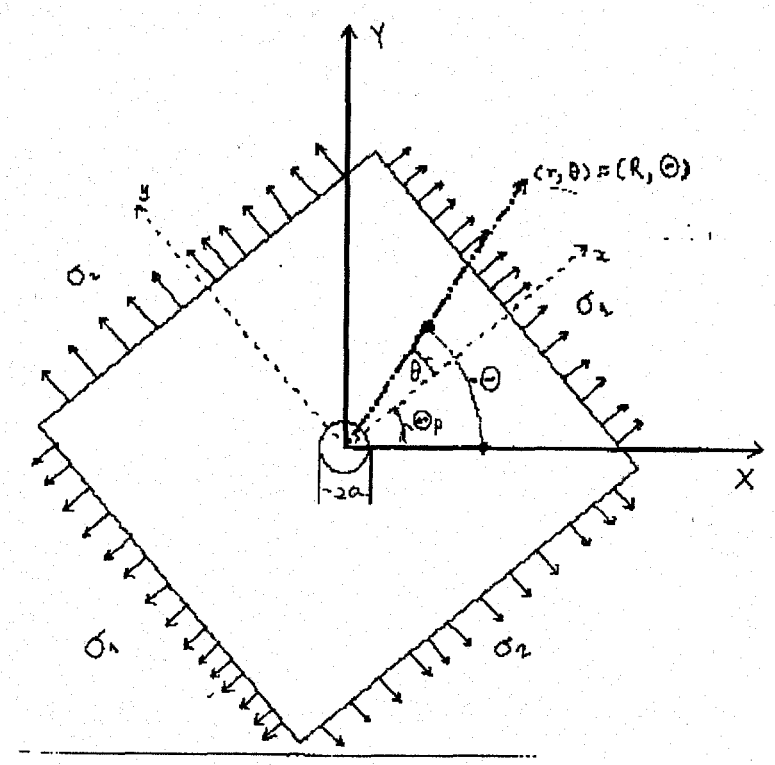

$$\sigma_r = \frac{\sigma_1 + \sigma_2}{2} + \frac{\sigma_1 - \sigma_2}{2}\text{Cos}2\theta \qquad 5.1$$

$$\sigma_\theta = \frac{\sigma_1 + \sigma_2}{2} + \frac{\sigma_1 - \sigma_2}{2}\text{Cos}2\theta \qquad 5.2$$

$$\tau_{r\theta} = -\frac{\sigma_1 - \sigma_2}{2}\text{Sin}2\theta \qquad 5.3$$

Hence the biaxial initial stress state of the residual stress (before the drilling of the hole) expressed in (R, Θ) system is given by:

$$\sigma_R = \frac{\sigma_1 + \sigma_2}{2} + \frac{\sigma_1 - \sigma_2}{2} \mathrm{Cos2}(\Theta - \Theta_p) \qquad 5.1^*$$

$$\sigma_\Theta = \frac{\sigma_1 + \sigma_2}{2} - \frac{\sigma_1 - \sigma_2}{2} \mathrm{Cos2}(\Theta - \Theta_p) \qquad 5.2^*$$

$$\tau_{R\Theta} = -\frac{\sigma_1 - \sigma_2}{2} \mathrm{Sin2}(\Theta - \Theta_p) \qquad 5.3^*$$

After the hole is drilled, the resulting stress field σ'' is the Kirsch solution for a biaxial loaded infinite plate. The Kirsch solution in (r, θ) system is given by:

$$\sigma_r'' = \frac{\sigma_1 + \sigma_2}{2}\left(1 - \frac{a^2}{r^2}\right) + \frac{\sigma_1 + \sigma_2}{2}\left(1 + \frac{3a^4}{r^4} - \frac{4a^2}{r^2}\right)\mathrm{Cos2}\theta \qquad 5.4$$

$$\sigma_\theta'' = \frac{\sigma_1 + \sigma_2}{2}\left(1 + \frac{a^2}{r^2}\right) - \frac{\sigma_1 - \sigma_2}{2}\left(1 + \frac{3a^4}{r^4}\right)\mathrm{Cos2}\theta \qquad 5.5$$

$$\tau_{r\theta}'' = -\frac{\sigma_1 - \sigma_2}{2}\left(1 - \frac{3a^4}{r^4} + \frac{2a^2}{r^2}\right)\mathrm{Sin2}\theta \qquad 5.6$$

The Kirsch solution in (R, Θ) system is given by:

$$\sigma_R'' = \frac{\sigma_1 + \sigma_2}{2}\left(1 - \frac{a^2}{r^2}\right) + \frac{\sigma_1 + \sigma_2}{2}\left(1 + \frac{3a^4}{r^4} - \frac{4a^2}{r^2}\right)\mathrm{Cos2}(\Theta - \Theta_p) \qquad 5.4^*$$

$$\sigma_\Theta'' = \frac{\sigma_1 + \sigma_2}{2}\left(1 + \frac{a^2}{r^2}\right) - \frac{\sigma_1 - \sigma_2}{2}\left(1 + \frac{3a^4}{r^4}\right)\mathrm{Cos2}(\Theta - \Theta_p) \qquad 5.5^*$$

$$\tau_{R\Theta}'' = -\frac{\sigma_1 - \sigma_2}{2}\left(1 - \frac{3a^4}{r^4} + \frac{2a^2}{r^2}\right)\mathrm{Sin2}(\Theta - \Theta_p) \qquad 5.6^*$$

By principal of super-positioning, subtracting the residual stress system before the hole is drilled (σ), from the residual stress system after the hole was drilled (σ'') yields the hole drilling released

stress(σ'), which can be shown graphically as follows Figure 5-2:

Figure 5-2 Schematic of Superposition of Residual Stress

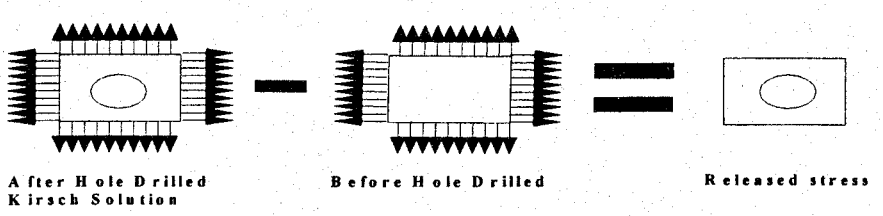

Mathematically, this is shown in equations as for the (r, θ) system:

$$\sigma_r' = \sigma_r'' - \sigma_r = -\frac{\sigma_1+\sigma_2}{2}\left(\frac{a^2}{r^2}\right) + \frac{\sigma_1-\sigma_2}{2}\left(\frac{3a^4}{r^4} - \frac{4a^2}{r^2}\right)\text{Cos}2\theta \qquad 5.7$$

$$\sigma_\theta' = \sigma_\theta'' - \sigma_r = -\frac{\sigma_1+\sigma_2}{2}\left(\frac{a^2}{r^2}\right) - \frac{\sigma_1-\sigma_2}{2}\left(\frac{3a^4}{r^4}\right)\text{Cos}2\theta \qquad 5.8$$

$$\tau_{r\theta}' = \tau_{r\theta}'' - \tau_{r\theta}' = -\frac{\sigma_1-\sigma_2}{2}\left(\frac{3a^4}{r^4} - \frac{2a^2}{r^2}\right)Sin2\theta \qquad 5.9$$

And for the (R, Θ) system,

$$\sigma_R' = \sigma_R'' - \sigma_R = -\frac{\sigma_1+\sigma_2}{2}\left(\frac{a^2}{R^2}\right) + \frac{\sigma_1-\sigma_2}{2}\left(\frac{3a^4}{R^4} - \frac{4a^2}{R^2}\right)\text{Cos}2(\Theta-\Theta_p) \qquad 5.7^*$$

$$\sigma_\Theta' = \sigma_\Theta'' - \sigma_\Theta = \frac{\sigma_1+\sigma_2}{2}\left(\frac{a^2}{R^2}\right) - \frac{\sigma_1-\sigma_2}{2}\left(\frac{3a^4}{R^4}\right)\text{Cos}2(\Theta-\Theta_p) \qquad 5.8^*$$

$$\tau_{R\Theta}' = \tau_{R\Theta}'' - \tau_{R\Theta} = \frac{\sigma_1-\sigma_2}{2}\left(1 - \frac{3a^4}{R^4} + \frac{2a^2}{R^2}\right)\text{Sin}2(\Theta-\Theta_p) \qquad 5.9^*$$

The raw data or known data are two normal strain components ($\varepsilon_X, \varepsilon_Y$) and a shear component of the release strain. The data are measured under the (X,Y) Cartesian system and its equivalent (R, Θ) system. The two principal residual stresses (σ_1, σ_2) and the orientation of the residual stress field Θ_p with respect to the pre-determined axis (X,Y) are the desired or unknown values.

Now it comes to the step to solve the residuals stress. From the definition of maximum shear stress:

$$\tau_m = \frac{\sigma_1 - \sigma_2}{2} \qquad 5.10$$

The average stress is defined as:

$$\sigma_a = \frac{\sigma_r + \sigma_\theta}{2} = \frac{\sigma_R + \sigma_\Theta}{2} \qquad 5.11$$

For the sake of simplification purposes:

$$\lambda = \frac{a}{r} = \frac{a}{R}$$

By adding equation 5.7* and 5.8* thus:

$$\tau_m = -\frac{\sigma_a^{'}}{2\lambda^2 \mathrm{Cos}2(\Theta - \Theta_p)} \qquad 5.12$$

Substituting equation 5.9* into A1 yields:

$$\theta = \Theta - \Theta_p = \frac{1}{2}\tan^{-1}\frac{4\tau_{R\Theta}^{'}}{(\sigma_R^{'} + \sigma_\Theta^{'})(2 - 3\lambda^2)} = \frac{1}{2}\tan^{-1}\frac{2\tau_{R\Theta}^{'}}{\sigma_a^{'}(2 - 3\lambda^2)} \qquad 5.13$$

By subtracting equations 5.7* and 5.8*

$$\sigma_R^{'} - \sigma_\Theta^{'} = -(\sigma_1 + \sigma_2)\lambda^2 + \frac{\sigma_1 - \sigma_2}{2}(6\lambda^4 - 4\lambda^2)\mathrm{Cos}2(\Theta - \Theta_p) \qquad 5.14$$

From equation A1, by substitution, it comes to:

$$\frac{\sigma_1 + \sigma_2}{2} = -\frac{3}{4}\sigma_R^{'} - (\frac{3}{4} - \lambda^2)\sigma_\Theta^{'} = -\frac{3}{4}\sigma_a^{'} + \frac{\sigma_\Theta^{'}}{\lambda^2} \qquad 5.15$$

As a result, the residual stress components $\tau_m, \sigma_a, \Theta_p$ are now all written in term of the hole drilling released stress components in the (R, Θ) system:

$$\tau_m = -\frac{\sigma_a^{'}}{2\lambda^2 \mathrm{Cos}2(\Theta - \Theta_p)} \qquad 5.16$$

$$\sigma_a = -\frac{3}{4}\sigma_a^{'} + \frac{1}{\lambda^2}\sigma_\Theta^{'} \qquad 5.17$$

$$\Theta_p = \Theta - \frac{1}{2}\tan^{-1}\frac{\tau_{R\Theta}^{'}}{\sigma_a^{'}(2 - 3\lambda^2)} \qquad 5.18$$

But since the measured experimental values are in the (X,Y) system, it is necessary to rewrite the released strain components in terms of (X,Y) system. This is to be done by relating the released strain components in the (R, Θ) system to the (X,Y) system by strain transformation equations.

By 2-D Hooke's laws, A5 and A7 are rewritten in term of the released strains.

$$\tau_m = -\frac{\sigma_a^{'}}{2\lambda^2 \mathrm{Cos}2(\Theta - \Theta_p)} = -\frac{E}{2(1 - \nu)\lambda^2}\frac{\varepsilon_a^{'}}{\mathrm{Cos}2(\Theta - \Theta_p)} \qquad 5.19$$

$$\begin{aligned}\sigma_a &= -\frac{3}{4}\sigma_a^{'} + \frac{1}{\lambda^2}\sigma_\Theta^{'} = -\frac{3}{4}\frac{E}{1 - \nu}\varepsilon_a^{'} + \frac{E}{1 - \nu^2}\frac{1}{\lambda^2}(\nu\varepsilon_R^{'} + \varepsilon_\Theta^{'}) \\ &= \frac{E}{1 - \nu^2}\frac{1}{\lambda^2}\left\{\left[-\frac{3}{4}(1 + \nu)\lambda^2 + 2\right]\varepsilon_a^{'} - (1 - \nu)\varepsilon_R^{'}\right\}\end{aligned} \qquad 5.20$$

$$\Theta_p = \Theta - \frac{1}{2}\tan^{-1}\left[\left(\frac{(1-\nu)}{(1+\nu)}\right)\frac{\gamma'_{R\Theta}}{(2-3\lambda^2)\varepsilon'_a}\right] \qquad 5.21$$

So far, the residual stress components are related to the released strains in the (X,Y), from the following strain transformation equations:

$$\varepsilon'_R = \frac{\varepsilon'_X + \varepsilon'_Y}{2} + \frac{\varepsilon'_X - \varepsilon'_Y}{2}\mathrm{Cos}2\Theta + \frac{\gamma'_{XY}}{2}\mathrm{Sin}2\Theta$$

$$\varepsilon'_\Theta = \frac{\varepsilon'_X + \varepsilon'_Y}{2} - \frac{\varepsilon'_X - \varepsilon'_Y}{2}\mathrm{Cos}2\Theta - \frac{\gamma'_{XY}}{2}\mathrm{Sin}2\Theta$$

$$\gamma'_{R\Theta} = -(\varepsilon'_X - \varepsilon'_Y)\mathrm{Sin}2\Theta + \gamma'_{XY}\mathrm{Cos}2\Theta$$

$$\varepsilon'_a = \frac{\varepsilon'_R + \varepsilon'_\Theta}{2} = \frac{\varepsilon'_X + \varepsilon'_Y}{2}$$

So equations A8 and A10 come to:

$$\tau_m = -\frac{E}{2(1-\nu)}\frac{\varepsilon'_a}{Cos2(\Theta - \Theta_p)} \qquad 5.22$$

$$\begin{aligned}\sigma_a &= -\frac{3}{4}\sigma'_a + \frac{1}{\lambda}\sigma'_\Theta \\ &= -\frac{3}{4}\frac{E}{1-\upsilon}\varepsilon'_a + \frac{E}{1-\upsilon^2}\left(\upsilon\varepsilon'_R + \varepsilon'_\Theta\right) \\ &= \frac{E}{1-\upsilon^2}\frac{1}{\lambda^2}\left\{\left[-\frac{3}{4}(1+\upsilon)\lambda^2 + 2\right]\varepsilon'_a + (\upsilon - 1)\varepsilon'_R\right\}\end{aligned} \qquad 5.23$$

$$\Theta_p = \Theta - \frac{1}{2}\tan^{-1}\left[\left(\frac{1-\nu}{1+\nu}\right)\frac{\gamma_{R\Theta}}{(2-3\lambda^2)\varepsilon'_a}\right] \qquad 5.24$$

$$= \Theta - \frac{1}{2}\tan^{-1}\left[\left(\frac{1-\nu}{1+\nu}\right)\frac{-(\varepsilon_X' - \varepsilon_Y')Sin2\Theta + \gamma_{XY}' Cos2\Theta}{(2-3\lambda^2)\dfrac{\varepsilon_X' + \varepsilon_Y'}{2}}\right]$$

$$= \Theta - \frac{1}{2}\tan^{-1}\left[\left(\frac{1-\nu}{1+\nu}\right)\frac{(\varepsilon_X' - \varepsilon_Y')Sin2\Theta - \gamma_{XY}' Cos2\Theta}{(\frac{3}{2}\lambda^2 - 1)(\varepsilon_X' + \varepsilon_Y')}\right]$$

Hence the initial principal residual stresses are obtained as

$$\sigma_2 = \tau_m + \sigma_a$$

$$\sigma_1 = \sigma_a - \tau_m$$

$$\sigma_1 = \frac{E}{1-\nu^2}\frac{1}{\lambda^2}\left(\left[-\frac{3}{4}(1+\nu)\lambda^2 + 2\right]\frac{\varepsilon_x' + \varepsilon_y'}{2} - \frac{(1-\nu)}{2}\left[\varepsilon_x' + \varepsilon_y' + (\varepsilon_X' - \varepsilon_Y')Cos2\Theta + \frac{\gamma_{XY}'}{2}Sin2\Theta\right]\right) + \frac{E}{2(1-\nu)}\frac{\varepsilon_a'}{Cos2(\Theta - \Theta_p)}$$

$$\sigma_2 = \frac{E}{1-\nu^2}\frac{1}{\lambda^2}\left(\left[-\frac{3}{4}(1+\nu)\lambda^2 + 2\right]\frac{\varepsilon_x' + \varepsilon_y'}{2} - \frac{(1-\nu)}{2}\left[\varepsilon_x' + \varepsilon_y' + (\varepsilon_X' - \varepsilon_Y')Cos2\Theta + \frac{\gamma_{XY}'}{2}Sin2\Theta\right]\right) - \frac{E}{2(1-\nu)}\frac{\varepsilon_a'}{Cos2(\Theta - \Theta_p)}$$

$$\Theta_p = \Theta - \frac{1}{2}\tan^{-1}\left[\left(\frac{1-\nu}{1+\nu}\right)\frac{(\varepsilon_X' - \varepsilon_Y')Sin2\Theta - \gamma_{XY}' Cos2\Theta}{(\frac{3}{2}\lambda^2 - 1)(\varepsilon_X' + \varepsilon_Y')}\right]$$

Conclusion

Based on the Kirsch solution and the method of superposition, the unknown residual stress can be expressed in the term of released strain components which is obtainable from the DSC method. That is to say, once DSC is operated and the released strain component is measured, just plug in the provided equation, the residual stress can be determined.

Chapter 6 DSC Measurement Factors Analysis and Determination

It has been known that the hole drilling method is rapid and versatile. Still, there are some limitations and the accuracy is needed to be examined and improved. Therefore, details of influential parameters and factors will be discussed upon which the conclusion is drawn.

6.1 DSC measurement range determination

One of the accuracy concerns of the hole-drilling method is directly related to the ability of locating the hole accurately in the centre of the rosette. As an example, if the hole is no more that 0.001" off centre, the residual strain error is less than 3%. In the practice, it will be more than that. Thus, lots of care should be taken in order to have an accurate result when applying hole-drilling method to measure the residual stress.

The standard hole drilling method procedures including measurement range and depth of the drilled hole in ASTM 387 will be examined. Afterward, it will be applied to DSC method because the two methods essentially same, except for the different strain-capture tools.

The common procedure for measuring the relieved strains is to mount three resistance strain gages in the form of a rosette around the site of the hole before drilling. Such a rosette is shown schematically in Figure 6-1, where three radically oriented strain gages are located with their centers at the radius R from the center of the hole.

Figure 6-1 Schematic of Strain gage

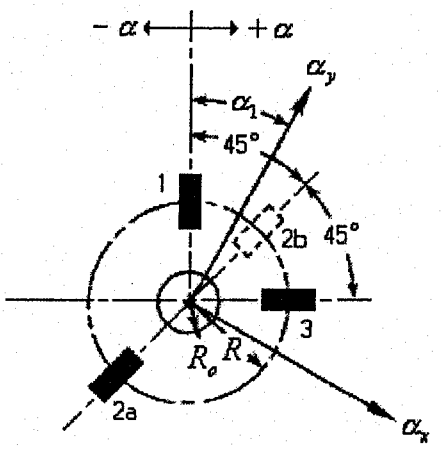

Although the angles between gages can be arbitrary (but must be known), a 45-degree angular increment leads to the simplest analytical expressions, and thus has become the standard for commercial residual stress rosettes.

In the DSC measurement, the ideal range area should be, logically, a radical band around the drilled hole, while the location range should be theoretically and experimentally found.

The relieved strains generally decrease with increasing distance from the hole increases. Because of this, it is desirable to measure the strains close to the edge of the hole in order to maximize the strain gage output signal. Against the will, plasticity effects also increase in the immediate vicinity of the hole. These considerations, along with practical aspects of strain gage design and application, necessitate a compromise in selecting the optimum radius (R) for gage location. Analytical and experimental studies have established a practical range of $0.3 < r < 0.45$ where $r = R_o / R$ and R_0 is the radius of the hole and R is the radius to the longitudinal centre of the gage.

So there is the practical range in term of the hole diameter is from $R_0/0.45$ to $R_0/0.3$, that is 1.11D to 1.67 D, where D in the diameter of the drilled hole. Based on the ASTM E837, there are three types of commonly used hole diameters available and shown in Table 6-1 as follows:

Table 6-1 Three Types of Hole Diameter

Type A	Type B	Type C
1.01mm	2.54mm	2.54mm
2.54mm	N/A	N/A
5.89mm	N/A	N/A

To be noted that in the ASTM, the minimum recommended hole diameter is 60% of the maximum allowable diameter. In light of the different material properties, the diameter of the hole can be different. In order to avoid to missing the possible value, it would like to cover more range area than the smaller one. Therefore, here only the maximum value is considered.

Based on the calculated range, it is possible to calculate the specific range with respect to one specific hole. Table 6-2 contains the both hole diameter and recommended range in unit of millimetre.

The table can be used as recommendation, while as to the specific problems, the range can be adjusted on the trial and error basis.

Table 6-2 Recommended Hole Diameter and Measurement Range

Type A Diameter	DSC measure Range to the centre of the hole	Type B Diameter	DSC measure Range to the centre of the hole	Type C Diameter	DSC measure Range to the centre of the hole
1.01mm	1.12-1.69	2.54mm	2.82-4.24	2.54mm	2.82-4.24
2.54mm	2.82-4.24	N/A	N/A	N/A	N/A
5.89mm	6.54-9.84	N/A	N/A	N/A	N/A

6.2 DSC Measurement Depth Determination

In general, the large holes are recommended because of the increased of sensitivity. Under an ideally condition, it is expected to drill a large hole, the sensitivity can be improved greatly. However, due to the nature of the method, it is still semi-destructive which means " It should be applied only in those cases either where the specimen is expendable or where the introduction of a small shallow hole will not significantly affect the usefulness of the specimen." [1] Therefore, it is possible to drill the hole as small as possible to meet this requirement. Consequently, it comes to the problem how to accurately determine the value of hole.

The general variation of relieved strain with depth is illustrated, where the strains have been normalized, in this case, to 100% at Z/D= 0.4. The data shown above include experimental results from two different investigators demonstrating the manner in which the relieved-strain function is affected by the ratio of hole diameter to gage circle diameter (D_o/D). Both cases involve uniform uniaxial (plane) stress, in specimens which are thick compared to the maximum hole depth. The curves plotted in the figure are considered representative of the response to be expected when the residual stress is uniform throughout the hole depth.

The above mentioned range is related with the hole radius. Thus it is highly possible that the empirical result also can be used in the DSC method because the study field is the same except the different measure method. In order to maximize the strain signals, the hole is normally drilled to a depth in corresponding to at least Z/D= 0.4 (ASTM E837 specifies Z/D= 0.4 for the maximum hole depth).

Once the range is determined, the possible hole depth range can be obtained as follows in Table 6-3:

Table 6-3 Hole Depth Range Of Three Different Gages

Type A Diameter	DSC measure Range to the centre of the hole	Hole depth range	Type B Diameter	DSC measure Range to the centre of the hole	Hole depth range	ype C iameter	DSC measure Range to the centre of the hole	Hole depth range
1.01	1.12-1.69	0.45-0.68	2.54	2.82-4.24	1.13-1.70	.54	2.82-4.24	1.13-1.70
2.54	2.82-4.24	1.13-1.70	N/A	N/A	N/A	N/A	N/A	N/A
5.89	6.54-9.84	2.60-3.94	N/A	N/A	N/A	N/A	N/A	N/A

The unit for each value in the table is millimeter. Gages types please refer to reference 2.

Although the argument has been raised that a blind hole was applicable, while the theory was developed for a through hole, which is not appropriate. To the author's understanding, it is applicable to apply this method on the blind hole because the higher value residual stress is close to the surface and the released strain is in the decreasing trend as the hole is drilled deeper, which can be proved theoretically and experimentally. So the close to the surface portion is under study so far.

Furthermore, by the theoretical and experimental method, even as to the sample which with residual stress uniform distribution and the released strains are measured by step by step hole drilling method. It shows the measured value of the first step is not the same as that of the followed step or the third. The deeper the hole is drilled, the smaller the value can be measured, which is the nature distribution of the residual stress.

Due to the various application and complex shape of the specimen, the blind hole has more applications than the through hole drilling. Therefore, it is feasible to apply this calculation in the blind hole drilling method.

6.3 Residual Stress Principal Direction Determination

From the strain graphics, Due to the nature of γ_{xy} and the equation [47]

$$\gamma'_{xy} = [A\tau_m + (\varepsilon'_x + \varepsilon'_y)]\tan 2\Theta \qquad 6.1$$

Where $A = \dfrac{(1+\upsilon)(6\lambda^4 - 4\lambda^2)}{E}$

when θ_p equals to 0, 90, 180 or 270 degree, γ_{xy} equals to 0, which is along with the principle axis. And the orientation of the residual stress field with respect to the pre-determined axis (X,Y) are the desired. This is agreeable and can be seen from the experiment result.

6.4 Convergence area in the stress graphics

It can be found that the convergence of stresses coming to the relative constant value between 140 and 160 pixels in all principal stress graphics which are referred from reference 47 . The graphics show principal stress verses distance from hole. And this range is taken as to be the value to be sought. Here comes the question why and how people choose it in between 140 and 160 pixels. From the obtained stress graphics, it has been found they are all different patterns to some extent. However, from each graphic it is noticed that there is a trend which showing the calculated values begin to converge and then showing the scattering phenomenon. So it has been taken as the specific period under study.

The reason that it comes to scatter after certain distance or value can be explained that the relieved stress is inverse to the distance to the hole centre. The uneven and unpredictable value appeared before the convergence can probably be explained that due to the plasticity effect when drilling the hole and

the influence from the material itself.

Discussion

In the part of DSC measurement factors determination, it is known the DSC measurement range determination, DSC measurement Depth determination, θ_p determination and convergence area in the stress graphics. It should be noted that it can be achieved by DSC method a whole field of value in form of contour map compared to the strain gage that only single value can be measured. Therefore, the shortcut to find the most significant value in order to reducing the relatively great calculation is needed to be done.

In the hole drilling method, the different drills are provided by ASTM. The feature of them is discussed. In aiming to drilling the smallest hole, it is proposed by author laser drill can be used. By taking advantage of the laser, the method can be easily control special in the step by step measurement, greatly reduce the diameter of the hole and off-centre tolerance can be minimized substantially compared with other drills. Consequently, the related factors such as measurement range and hole depth are needed to carefully proceeded so as to get the accurate result.

The current application area of the DSC method is limited by its set-up meaning only can be performed in the lab. Comparing to the standardized method such as hole drilling method, it can be implemented on site which improves the feasibility and bring the diversity. From the history point of view, along the knowledge and technology improvement, no wonder it is expectable to see the portable DSC appearing in the working front line.

6.5 Full Coverage of Measurement Field

It is desirable to ensure γ_{xy} occurring when measuring. When there is a gap between the two neighboring graphics, the possibility exists that γ_{xy} passes right through the gaps, which means it can result no γ_{xy} value obtain from the experiment. This special case can be shown simplicity as

followed in Figure 6-2:

Figure 6-2 Missing γ_{xy} Condition

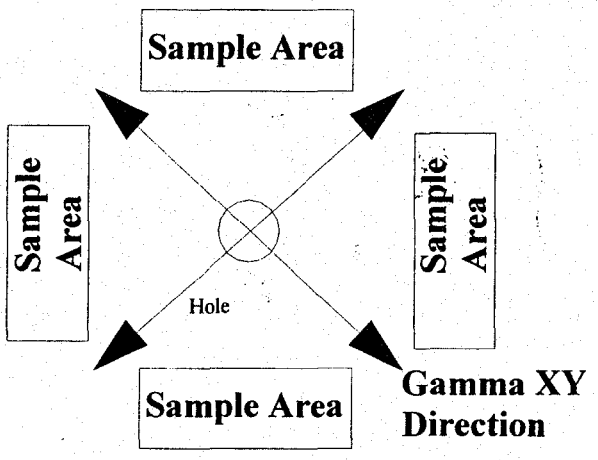

So it is recommend by author that it can have the four graphics overlaps to each other in order to avoid of the above- mentioned situation. The recommended one is shown below Figure 6-3:

Figure 6-3 Recommended Data Gathering Graphic

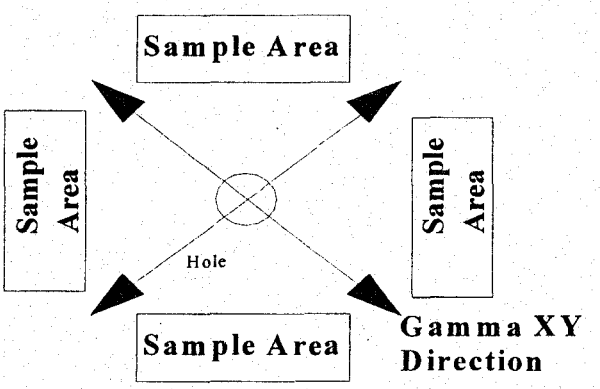

Conclusion

When applying DSC method in measuring the release strain, then determining the residual stress through the relevant equations, there are many factors needed to be considered. Because of natural feature of the hole drilling method itself, the measurement dimension such as the distance to the hole center and drilling depth are to be well-calculated and optimized. The ultimate goal is to provide assistance and help for the users, minimize the error and mature the method.

Chapter 7 Analysis and Discussion

Based on the proceeded chapter work, it has been established the relationship between the released strains and the residual stress. For the purpose of convenience, they are herein presented again.

$$\tau_m = \frac{\sigma_1 - \sigma_2}{2}$$

$$\tau_m = -\frac{E}{2(1-\nu)} \frac{\varepsilon_a'}{Cos2(\Theta - \Theta_p)} \tag{7.1}$$

$$\sigma_a = \frac{E}{1-\nu^2} \frac{1}{\lambda^2} \left(\left[-\frac{3}{4}(1+\nu)\lambda^2 + 2 \right] \varepsilon_a' - (1-\nu) \right) \varepsilon_R' \tag{7.2}$$

$$\Theta_p = \Theta - \frac{1}{2} \tan^{-1} \left[\left(\frac{1-\nu}{1+\nu} \right) \frac{(\varepsilon_X' - \varepsilon_Y') Sin2\Theta - \gamma_{XY}' Cos2\Theta}{(\frac{3}{2}\lambda^2 - 1)\varepsilon_X' + \varepsilon_Y'} \right] \tag{7.3}$$

It can be found that $\sigma_1 - \sigma_2 = 2\tau_m$, from the equation 7.1, for the purpose of simplicity,

$$\sigma_1 - \sigma_2 = N_1(\varepsilon_X' + \varepsilon_Y')$$

$$(\varepsilon_X' + \varepsilon_Y') = \frac{\sigma_1 - \sigma_2}{N_1} \tag{7.4}$$

Where $N_1 = -\frac{1}{2} \frac{E}{\upsilon} \frac{1}{\lambda^2 \cos 2(\Theta - \Theta_p)}$

Also from 7.3, it comes

$$\Theta_p = \Theta - \frac{1}{2}\tan^{-1}\left[\left(\frac{1-\nu}{1+\nu}\right)\frac{(\varepsilon_X^{'} - \varepsilon_Y^{'})Sin2\Theta - \gamma_{XY}^{'}Cos2\Theta}{(\frac{3}{2}\lambda^2 - 1)\varepsilon_X^{'} + \varepsilon_Y^{'}}\right]$$

$$2(\Theta - \Theta_p) = \frac{1}{2}\tan^{-1}\left[\left(\frac{1-\nu}{1+\nu}\right)\frac{(\varepsilon_X^{'} - \varepsilon_Y^{'})Sin2\Theta - \gamma_{XY}^{'}Cos2\Theta}{(\frac{3}{2}\lambda^2 - 1)\varepsilon_X^{'} + \varepsilon_Y^{'}}\right]$$

Perform tangent function on each side,

$$\tan 2(\Theta - \Theta_p) = \frac{1-\upsilon}{1+\upsilon}\frac{(\varepsilon_X^{'} - \varepsilon_Y^{'})Sin2\Theta - \gamma_{XY}^{'}Cos2\Theta}{(\frac{3}{2}\lambda^2 - 1)\varepsilon_X^{'} + \varepsilon_Y^{'}}$$

$$\gamma_{xy}^{'} = \tan 2\Theta(\varepsilon_x^{'} - \varepsilon_y^{'}) - \frac{(1+\upsilon)}{1-\upsilon}\frac{(1.5\lambda^2 - 1)\tan 2(\Theta - \Theta_p)(\varepsilon_x^{'} + \varepsilon_y^{'})}{\cos 2\Theta} \qquad 7.5$$

Furthermore, it is known that $\frac{\sigma_1 + \sigma_2}{2} = \sigma_a$

From equation 7.6,

$$\frac{\sigma_1 + \sigma_2}{2} = \frac{E}{1-\nu^2}\frac{1}{\lambda^2}\left(\left[-\frac{3}{4}(1+\nu)\lambda^2 + 2\right]\frac{\varepsilon_x^{'} + \varepsilon_y^{'}}{2} - \frac{(1-\nu)}{2}\left[\varepsilon_x^{'} + \varepsilon_y^{'} + (\varepsilon_X^{'} - \varepsilon_Y^{'})Cos2\Theta + \frac{\gamma_{XY}^{'}}{2}Sin2\Theta\right]\right)$$

Clear up and $\varepsilon_x^{'} - \varepsilon_y^{'}$ can be expressed in the following, named 7.6:

$$\varepsilon_x^{'} - \varepsilon_y^{'} = \frac{1}{\cos 2\Theta}\left\{\frac{(\varepsilon_x^{'} + \varepsilon_y^{'})\{2 - 0.75(1+\upsilon)\lambda^2\}}{1-\upsilon} - \frac{\lambda^2(1+\upsilon)(\sigma_1 + \sigma_2)}{E} - (\varepsilon_x^{'} + \varepsilon_y^{'}) - \sin 2\Theta\gamma_{xy}^{'}\right\}$$

...7.6

Now substitute equation 7.5 into to 7.6 and re-arrange, it comes:

$$\varepsilon_x^{'} - \varepsilon_y^{'} = \cos 2\Theta \,[\frac{(\varepsilon_x^{'} + \varepsilon_y^{'})\{2 - 0.75(1+\upsilon)\lambda^2\}}{1-\upsilon} - \frac{\lambda^2(1+\upsilon)(\sigma_1+\sigma_2)}{E} - (\varepsilon_x^{'} + \varepsilon_y^{'}) +$$

$$\frac{(\varepsilon_x^{'} + \varepsilon_y^{'})(1+\upsilon)(1.5\lambda^2 - 1)\tan 2\Theta \tan 2(\Theta - \Theta_p)}{1-\upsilon}] \qquad 7.7$$

Take equation 7.4 into 7.7 and it is named the clear- up equation 7.8, shown as follows:

$$\varepsilon_x^{'} - \varepsilon_y^{'} = \cos 2\Theta \,[\frac{\sigma_1 - \sigma_2}{N_1}\{\frac{\{2 - 0.75(1+\upsilon)\lambda^2\} + (1+\upsilon)(1.5\lambda^2 - 1)\tan 2\Theta \tan 2(\Theta - \Theta_p)}{1-\upsilon} -$$

$$1\} - \frac{\lambda^2(1+\upsilon)(\sigma_1+\sigma_2)}{E}] \qquad 7.8$$

The coming st(p is to sum the equations 7.4 and 7.8, at the mean time, take the expression of N_1 back, after clea up, yielding the following equation:

$$\varepsilon_x^{'} = \quad -\frac{\lambda^2(1-\upsilon)(\sigma_1 - \sigma_2)\lambda^2 c2(\Theta - \Theta_p)}{E} \bullet$$

$$\{1 + \cos 2\Theta[\frac{\{2 - 0.75(1+\upsilon)\lambda^2\} + (1+\upsilon)(1.5\lambda^2 - 1)\tan 2\Theta \tan 2(\Theta - \Theta_p)}{1-\upsilon} - 1]\}$$

$$- \frac{\lambda^2(1+\upsilon)(\sigma_1+\sigma_2)}{E} \qquad 7.9$$

From 7.4, easily it can be determined $\varepsilon_y^{'}$ as following:

$$\varepsilon_y^{'} = -\frac{\lambda^2(1-\upsilon)(\sigma_1 - \sigma_2)\lambda^2 c2(\Theta - \Theta_p)}{E} \bullet$$

$$\{1 - \cos 2\Theta[\frac{\{2 - 0.75(1+\upsilon)\lambda^2\} + (1+\upsilon)(1.5\lambda^2 - 1)\tan 2\Theta \tan 2(\Theta - \Theta_p)}{1-\upsilon} - 1]\}$$

$$+\frac{\lambda^2(1+\upsilon)(\sigma_1+\sigma_2)}{E} \qquad 7.10$$

Up to now, $\varepsilon_x^{'}, \varepsilon_y^{'}$ have been determined.

Just take the value into equation 7.4, it comes to equation 7.11

$$\gamma_{xy}^{'} = -4\frac{\sin 2\Theta \cos 2(\Theta-\Theta_p)(\sigma_1-\sigma_2)\lambda^2(1+\upsilon)\{1-0.75\lambda^2+(1.5\lambda^2-1)\tan 2\Theta \tan 2(\Theta-\Theta_p)\}}{E}$$

$$-\frac{2\tan 2\Theta(\sigma_1+\sigma_2)(1+\upsilon)\lambda^2}{E}+\frac{2(1+\upsilon)\lambda^2 \sin 2(\Theta-\Theta_p)(1.5\lambda^2-1)(\sigma_1-\sigma_2)}{E\cos 2\Theta} \qquad 7.11$$

So far it has been established the relationship between the released strain and the principal stress components in the polar coordinate with the variables of λ and θ. λ is the result of a/r, in which **a** stands for the radius of drilled hole; **r** stands for the distance from measured field to the hole center.

By using MathCad 8, the graphic has been plotted $\varepsilon_X^{'}, \varepsilon_Y^{'}, \gamma_{XY}^{'}$ in term of λ and θ. It is noted that when θ equals to θ_p or 90 degree different to θ_p, the $\varepsilon_X^{'}, \varepsilon_Y^{'}$ come to the greatest magnitude, while $\gamma_{XY}^{'}$ is zero. For this certain condition, its graphic is shown in Figure 7-1 enclosed which shows the greatest magnitude including plus and minus signs comes from θ equals to θ_p or 90 degree different to θ_p.

Figure 7-1

The graphic show the change of released strain
with respect to lambda (resulting value of drilled hole radius over distance from hole center to measurement field margin)and theta, which is in polor coordinate.

The specific conditions are given as follows:
Radius of drilled hole is a= 0.01m,
u = 0.3,
E = 100,
Measurement range
Theta changes from -90 degree to 90 degree,
Lambda from 0.5 to 0.75,
Sigma 1=0.5,
Sigma 2=0.01,
Theta p is 0 degree

It shows the greated magnitude comes along the principle direction. In this specifice condition, it is 0 degree.

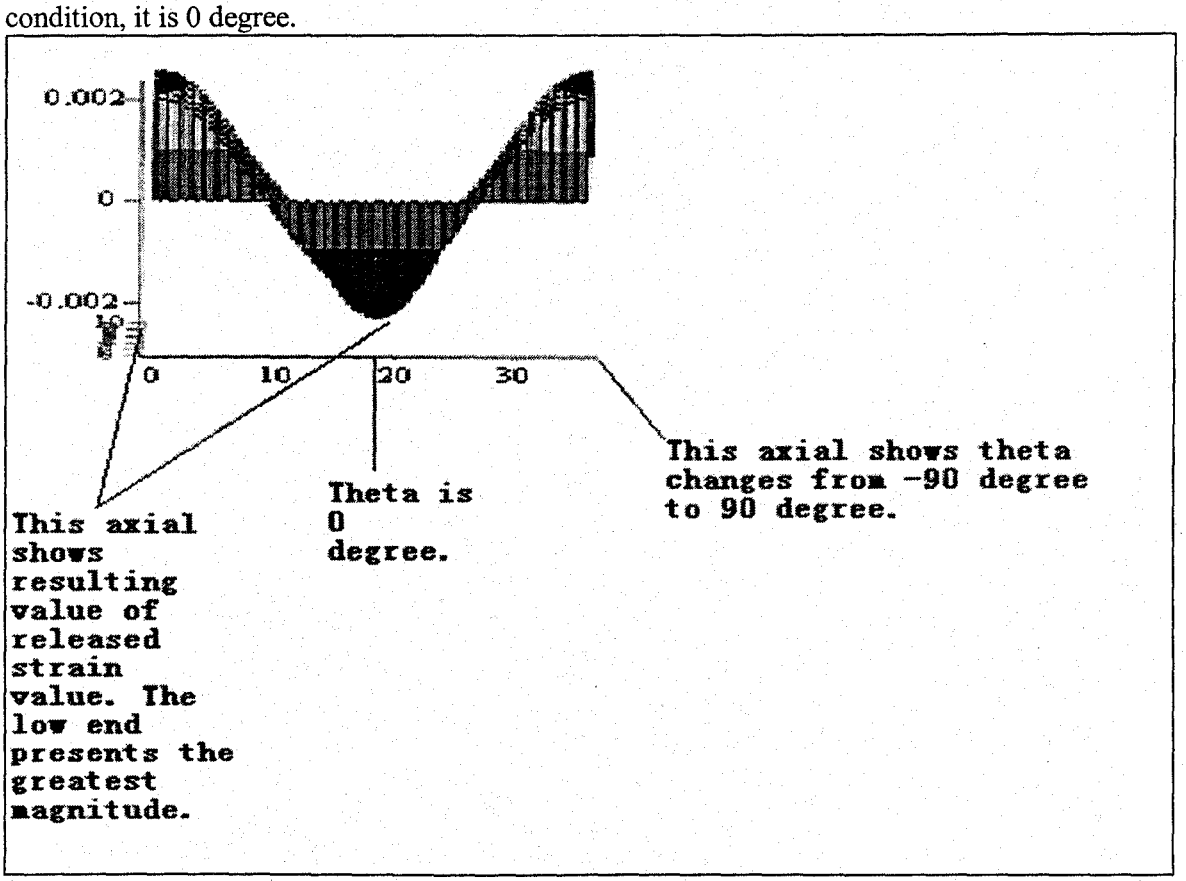

Analysis Part I

Firstly, in the coming experiment when determining value of θ_p, it has been known that along that θ_p direction or the principal direction, it can obtain the greatest magnitude value of $\varepsilon_X^{'}, \varepsilon_Y^{'}$ and zero value of $\gamma_{XY}^{'}$. When calculation, rather than plugging three different values $\varepsilon_X^{'}, \varepsilon_Y^{'}, \gamma_{XY}^{'}$ into the equations in determining the residual stress component such as σ_1, σ_2, only two values of $\varepsilon_X^{'}, \varepsilon_Y^{'}$ are suffice to obtain σ_1, σ_2 because of $\gamma_{XY}^{'}$ is zero at the moment. By doing so, the cost of calculation has been saved and it is one simple and consist way in determining the residual stress.

Secondly, there are many random errors existing in the DSC method. It is known that each of them make the contribution to the whole error system, while none of them has resulted in the major influence in the technique. Based on the knowledge of statistics knowledge, by comparing the greater and the smaller magnitude values, the error percent generated from greater magnitude is lesser than that of the smaller magnitude values. Therefore, from the error analysis point of view, the best way to reducing the level of the random error to the experiments result is to take the greatest magnitude for calculation. Based on the above analysis, the conclusion is drawn that determination of θ_p can both benefit to the reducing the calculation and errors generated from the system.

Analysis Part II

From the above analysis, initially it has been determined the principle direction of the residual stress for certain sample. Then, it is possible to rotate the identical specimen to that particular degree. When the proceeding hole is drilled, it is confidently expected that the residual stress principal direction is aligning with the system coordinates and the greatest magnitude value can be achieved along the direction.

Now it can be transformed from polar coordinate of the released strains and the residual stress equations into Cartesian coordinate, it can be expectable that it is capable to give us the visual contact that the relationship between the residual stress and released strain with the aid of MathCad 8.

The equations shown below provide the transformation from the polar coordinate to the Cartesian coordinate.

$$r = \sqrt{x^2 + y^2}$$
$$\theta = \tan^{-1}\frac{y}{x} \qquad 7.12$$

$$\lambda = \frac{a}{r} = \frac{a}{\sqrt{x^2 + y^2}} \qquad 7.13$$

So when plugging the above equations 7.12 and 7.13 into 7.9, 7.10 and 7.11, it comes to equation

$\varepsilon_x^{'}, \varepsilon_y^{'}$ and $\gamma_{xy}^{'}$ in term of x and y in Cartesian system.

Further, from the previous chapter's conclusion, it is known that the ideal hole radius. Here for example r =1 mm, and the measurement range is chosen according to the optical range which is discussed in the previous chapter.

By using MathCad 8, based on the above derived equations, in Cartesian coordinates the visual contact has been established, referring to Figure 7-2 enclosed, the function of the released strain components $\varepsilon_X^{'}, \varepsilon_Y^{'}, \gamma_{XY}^{'}$ in term of the residual stress components σ_1, σ_2.

Figure 7-2

The graphics show the values or patterns of released strain change with respect to changing of residual stress ratio.
The specific conditions are given as follows:
Radius of drilled hole is a= 0.01m,
Principle direction theta p is chosen as 0 degree,
u = 0.3,
E = 100,
Range of Measurement Area
X direction is from 0.2m to 0.6m,
Y direction is from +0.25m to -0.25m,
Sigma 1=0.5,
Sigma 2=0.25 ,
The residual stress ratio of 2:1 in the first grpahic, ratio of 5:1, 10:1 and 20:1 in the second, third and fourth graphics.

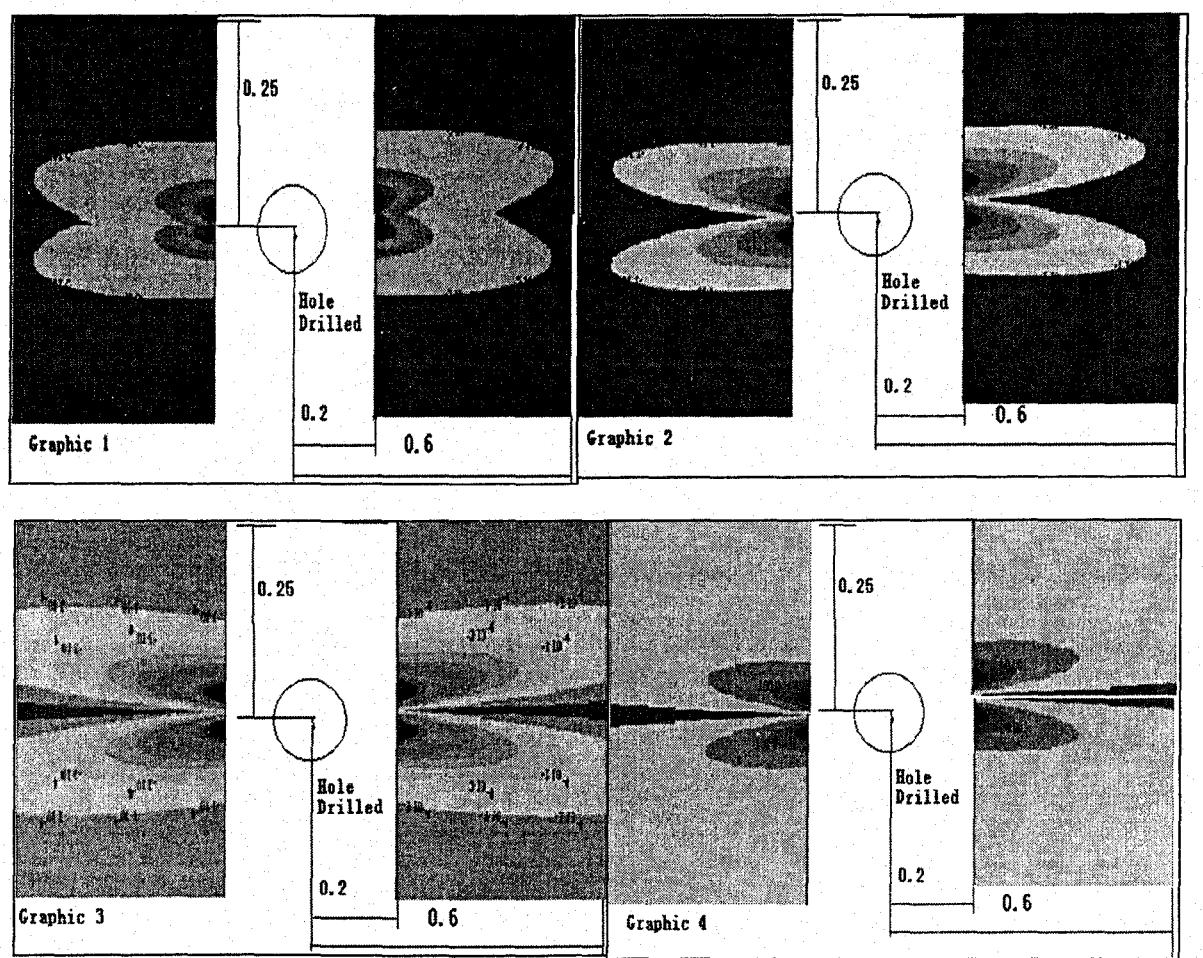

Intentionally by changing the ratio within the reasonable range, correspondently the contour map changes. Please refer to Figure 7-2 enclosed for different ratios and the graphics respectively. The graphics show that under the condition of the identical property samples and the same distance from the measured field to hole center on the right side for example, the patterns of the released strain vary correspondently when the principle stress ratio changes.

Furthermore, once the certain pattern change can be noticed and concluded, at the time of a fresh experiment is to be done, it can get to the ideas of the principle stress ratio which can be determined from the released strain patterns. It can provide the way to better understand the meaning of the released strains graphics.

Conclusion

In this chapter, by re-arranging the previous equation, it has been set up relationship between the released strain and residual stress. By using MathCad 8, the visual contact can be made. Furthermore, by acknowledging the understanding the change of contour map with the residual stress ratio, the understanding of residual stress and the released strain can be done.

Chapter 8 Conclusions

Extensive case studies have been examined and analyzed, so as to show that residual stress can be induced intentionally and unintentionally. As to determine the residual stress, various quantities and qualitative methods have been introduced, which can be distinguished between destructive techniques and the non-destructive techniques.

Digital Speckle Correlation (DSC) is a computerized method which determines the displacement, strains and consequently calculates the stress. The advantage of using DSC is shown and the limited of the method is discussed as well.

As to the DSC method, the parameters and factors including range determination, depth determination, principal direction determination, convergence area in the stress graphics and full coverage of measurement field have been examined. Further, the recommendation is given so as to provide the better solution for the method.

Based on the Kirsch solution, the equations related between the biaxial residual stress to the released strain components have been derived. Consequently, the relationship between the released strain and residual stress has been established.

With the aid of MathCad 8, it is acknowledged that that determination of principal direction can both benefit to the reducing the calculation and to the error brought to the system. Further, based on the visual contact to the changed patterns in the graphics when the residual stress ratios change, it can provide the way to better understand the meaning of the released strains graphics.

Reference:

[1] Handbook of Measurement of Residual Stress Edited by Jian Lu

[2] Mechanical metallurgy / George E. Dieter. New York : McGraw-Hill, c1986

[3] Residual stress effects on the fatigue life fan externally grooved thick-walled pressure vessel Song-In Lee, Seung_kee Kon; Prssure Vessel and Piping, 79(2002)119-126

[4] PuSL, Hussain MA Residual stress redistribution caused by notched and cracks in a partially autofretage tube, J Pressure Vessel Technol 1981; 103 :302-6

[5] Residual stress fields and fatigue analysis of autofrettaged parts by Thumser, J.W Bergmanaa, M Vormwald; Pressure vessels and Piping; 79 (2002) 113-117;

[6] Effect of expansion technique and plate thickness on near-hole residual stresses and fatigue life of cold expanded hole by A.T Oxdemir; Journal of Material Science 34 (1999) 1243-1252;

[7] The effect of cold expansion on fatigue crack growth from open holes at room and high temperature by V. D Lacarac KJ Smith, M, J Pavier; International Journal of Fatigue 23 (2001) S161-S170;

[8] Life enhancement of fatigue-aged fastener holes using the cold expansion process by J Gaeke, X Zhang and Z Wang,

[9] Sleeve cold working fastener holes by Phillips J L Air Force Materials Laboratory Report AFML-TR-74-10 Vol 1, 1974

[10] Thermal relaxation in autofrettaged cylinders by Kula E; proceeding of residual stress and stress relaxation 1982, 205-206;

[11] Kobayahsi M, matsui T, Murakami Y. Mechanism of creation of compressive residual stress by shot peening Int J Fatigue 1998; 20(5):351-7

[12] Residual stress state behavior under fatigue loading in pipeline welded joints by P Cindra Fonseca, JR teodosio, J Rebello and A Correia da Cruz;Journal of strain analysis Vol 36 No. 5

[13] Schiffner K, Helling CD. Simulation of residual stressed by shot peening 1999;72;329-40

[14] Li JK, Zhang R Yao M Computer simulation of residual stress field introduced by shot-peening; ICRS3 :1991;1284-89

[15] An evaluation of shot peening, residual stress and stress relaxation on the fatigue life of AISI 4340 steel by MAS Torres and HJC Voorwald; International Journal of Fatigue 24 (2002)877-886

[16] Wang S et al, Compressive residual stresses introduced by shot peening J mater Process Technol 1998;73 :64-73

[17] Li JK Zhang R, Yao M Experimental study on the compressive residual stress field introduced by shot peening ICRS3 : 1991;750-57

[18] Surface prestressing to improve fatigue strength of components by laser shot peening by G Hammersley, LA Hackel and F. Harris; Optics and Lasers in Engineering 34 (2000)327-337;

[19] Clauer, A. H., et al., 1981, "Effects of laser induced shock waves on metals," Shock Waves and High Strain Phenomena in Metals-Concepts and Applications, New York, Plenum, 1981, pp. 675-702

[20] Fabbro, R., et al., 1990, "Physical study of laser-produced plasma in confined geometry," J. Appl. Phys., July, 1990, Vol. 68(2), pp. 775-784.

[21] Meyer, L. W., 1992, "Constitutive equations at high strain rates," Shock-wave and High-Strain-Rate Phenomena in Metals, Marcel Dekker, Inc., New York, 1992, pp. 49-68.

[22] Laser shock processing of aluminum alloys application to high cycle fatigue behavior by P Peryre, R Fabbro, P Merrien and HP Lieurade Materials Science and Engineering A 210 (1996) 102-113;

[23] Laser-shock processing of aluminum-coated 55C1 steel in water –confinement regime, characterization and application to high-cycle fatigue behavior by P Peyre, L Berthe, X Scherpereel, R Fabbro, Journal of Materials Science 33 1999 1421-1429;

[24] Mechanical metallurgy / George E. Dieter. New York : McGraw-Hill, c1986 Page 410,

[25] Mathar "Determination of initial stresses by measuring the deformation around drilled holes"

[26] Rendler, N.J. and I. Vigness, "Hole-drilling Strain-gage Method of Measuring Residual Stresses." Proc., SESA XXIII, No. 2: 577-586 (1966).

[27] Schajer, G.S., "Application of Finite Element Calculations to Residual Stress Measurements." Journal of Engineering Materials and Technology 103: 157-163 (1981)

[28] G. Montay. A Cherouat, J, Lu "Development of the high precision incremental step hole drilling method for the study of residual stress in multi layer materials: influence of temperature and substrate on Zro2-Y2O3 8 wt% coatings"

[29] Roy. G "Residual stress determination by the hole drilling method: theory and applications"

[30] Roy.G "Determination of residual stress states in HY80 and HY100 plates by Neutron-diffraction, X-ray-diffraction, hole-drilling and numerical method

[31] Wang,Jia-yong "Measurements of residual stress by the hole drilling method: general stress strain relationship and its solution" Experimental mechanics, December 1988

[32] K. Sasaki, M Kishid and T, Itoh "The accuracy of residual stress measurement by the hole-drilling method"

[33] ASTM standard test method for "Determining residual stresses by the hole drilling strain gage method"

[34] Lu,j and Favenot JF, "Applications of the incremental hold-drilling method for measurement of residuals stress distribution." Experimental techniques Nov 1989

[35] Li. GD, Liu, BL and Li, BY "influence of the hole side plastic deformation as a result

stressconcentration on the accuracy of residual welding measurement by small blond hole relaxation method and its modification."

[36] G.S Schajer ad L. Yang Residual stress measurement in Orthotropic material by the hole drilling method

[37] On the measurement of Residual-stress Gradients in Aluminums-ally Specimens by Am, Nawwar and J, Shewchuk

[38] S Schajer and M Tootoonian "A new Rosette design for more reliable hole drilling residual stress measurements."

[39] Michael. T Flaman "Brief Investigation of Induced drilling stressed in the centre-hole method of residual-stress measurement"

[40] G. S. Schajer and L. Yang, "Residual-stress Measurement in Orthotropic Materials Using the Hole-drilling Method," Experimental Mechanics, Vol. 34, 12, December 1994, pp. 324- 333

[41] Residual stress distributions and their influence on fatigue lifetime

[42] Digital Image Correlation Using Newton-Raphson Method of Partial Differential Correction by H.A. Bruck, S.R. McNeil, M.A. Sutton and W.H. Peters III

[43] Feasibility of Digital Image Correlation Using Newton-Raphson Method of Partial Differential Correction by John Lansdale

[44] Randy L and Sue Ellen Haupt Practical Genetic Algorithms John Wiley & Sons Inc

[45] Botello, Marroguin, Onate and Van Horebeek Solving Structural Optimization Problems with Genetic Algorithm and Simulated Annealing, International Journal For Numerical Methods in Engineering

[46] Measurements Group, 1993, "Measurement of Residual stresses by the Hole-Drilling Strain Gage Method," North Carolina

[47] Investigation of the Residual stress using hole drilling method and digital speckle correlation by Luay Hussein